Data-Driven Spatio-Temporal Filters for Crosstalk Reduction in High-Density Surface EMG

IEEE Access
Multidisciplinary | Rapid Review | Open Access Journal

Received 7 February 2026, accepted 23 February 2026, date of publication 3 March 2026, date of current version 6 March 2026.

Digital Object Identifier 10.1109/ACCESS.2026.3669945

RESEARCH ARTICLE

Data-Driven Spatio-Temporal Filters for Crosstalk Reduction in High-Density Surface EMG

LUCA MESIN
Mathematical Biology and Physiology Research Group, Department of Electronics and Telecommunications, Politecnico di Torino, 10129 Turin, Italy
e-mail: luca.mesin@polito.it.

ABSTRACT Objective: Spatial filters have been extensively studied to improve selectivity of information extraction from high density surface electromyography (HD-EMG). However, variations in volume conductors and experimental conditions require tailored solutions, that predetermined filters with fixed weights cannot guarantee to be optimal. This work proposes the development of data-driven filters, adapted to the specific subject and experimental conditions, with a focus on crosstalk. Methods: A general framework to develop filters is introduced. The data are partitioned into patches, which the filter linearly combines across both electrode channels and time samples (obtaining a spatio-temporal filter). With the purpose to reduce crosstalk, different objective functions are proposed: maximal local correlation with the input and minimal cross-correlation across the output channels; minimum entropy of the filter output. Both optimization strategies promote sparse and spatially localized outputs, thereby reducing the effect of distant sources generating crosstalk. Results: Simulated monopolar HD-EMGs from two close muscles have been used to test the filters on a benchmark (n =60: 10 simulated subjects, 3 fat layer thicknesses, 2 levels of additive noise). Moreover, experimental data from selective contractions of the flexor carpi radialis and the pronator teres were used as a preliminary validation in the field (8 subjects). All proposed filters reduced the spread of the recorded signal, better focusing on the sources below the detection point. The estimation of the envelopes of the target muscles (i.e., the muscles located under the detection points of the filters) and the signal-to-crosstalk ratio were statistically improved in simulations when using the filters instead of the raw data. These positive outcomes were confirmed by trends observed in the experimental tests; however, the limited size of the dataset resulted in only a small number of statistically significant improvements. Conclusion: Defining a filter by optimizing an objective function allows to target a property of interest while adapting to the specific recording condition. This adaptive, data-driven approach offers a versatile tool for information extraction from HD-EMGs and may open new avenues for the investigation of neuromuscular signals.

INDEX TERMS Surface EMG, crosstalk, spatial filter, data-driven.

I. INTRODUCTION

Surface electromyogram (EMG) is recorded on the skin over a muscle during its contraction and reflects the bioelectric signals occurring when its motor units (MU) are activated [1]. The volume conductor spreads the potential generated by the bioelectric sources at the muscle fibers (i.e., the transmembrane currents), so that the resulting interference EMG includes the mixture of multiple overlapping MU action potentials (MUAP) that are difficult to separate. With the advent of multi-channel, high density surface EMG (HD-EMG), more information can be recorded from different locations, enabling a more detailed characterization of the neuromuscular activity underlying the recorded signals. Electric potentials from different electrodes have been combined by spatial filters: with their high-pass spatial frequency response, they can partially compensate for the low-pass diffusing effect of the volume conductor, providing a more

The associate editor coordinating the review of this manuscript and approving it for publication was Muammar Muhammad Kabir.

selective information on the underlying muscle activity. Different spatial filters have been introduced and studied both in simulated [2], [3], [4], [5], [6] and experimental conditions [7], [8], [9], [10], [11]. A filter is typically selected or evaluated based on key objectives it is intended to meet: for example, increasing the selectivity by focusing on a small detection volume, reducing the effect of non-propagating components (e.g., the end-of-fiber effect), improving the longitudinal selectivity (i.e., producing shorter MUAPs) in order to get a more precise timing of activation and separate contributions of different MUs [12]. However, advanced simulation models indicated the need to adapt to the investigated conditions [13], [14], as the specific details of the volume conductor (geometry and conductivity of different tissues [15], [16], [17], [18]) and recording condition (e.g., location with respect to the innervation zone (IZ) and tendons [19], orientation with respect to the muscle fibers [20]) deeply affect the results.

The improved selectivity of spatial filters with respect to the monopolar detection can contrast crosstalk [21], i.e., a signal from surrounding muscles which is superimposed to that from the target muscle of interest [22], [23]. In fact, electrodes used for surface EMG often have a wide detection volume [24], [25], so that they can pick up also signals produced by other muscles than that of interest. This unwanted interference remains an unsolved issue in surface EMG. It is challenging both to quantify and to suppress, and it can compromise various applications, including gait analysis [26], myoelectric prosthesis control [27], [28], [29], and ergonomic assessment [30].

Crosstalk have been studied both using simulations [2], [3], [4], [5], [6] and experimental measurements [7], [8], [9], [10], [11], [31]. Results consistently indicate the difficulty in measuring and mitigating crosstalk: for example, cross-correlation between EMG signals from target and non-target muscles does not reliably indicate signal quality [32]; the performance of spatial filters varies with the volume conductor [2]; simple temporal filtering fails to attenuate the problem [33].

The most common approaches to reduce crosstalk are to carefully select electrode placement [34] and apply spatial filtering [7], [9]. Such filters can suppress non-propagating components [35], [36], which are a primary contributor to crosstalk [37]. Nevertheless, their efficiency is influenced by several factors, including electrode type and size, tissue properties, and individual anatomy [2], [3], [4], [5], [6]. Moreover, they probe only a small detection volume, which may limit the representativeness of the signal [38].

Some methods have been introduced to tailor the information extraction to the specific application: the Optimal Spatio-Temporal Filter (OSTF) emphasizes the energy of the signal of interest while reducing that of disturbances (with possible application to crosstalk reduction) [39]; the non-linear spatio-temporal filter (NLSTF) has been introduced to estimate a bipolar EMG from noisy data corrupted by crosstalk [40]; inverse modelling can also help to estimate the signal from the muscle of interest [37], [41]. However, these methods are often cumbersome and demand preliminary investigations prior to application, such as recordings under selective conditions or detailed anatomical assessments. Other methods, based on decomposition algorithms [42], [43] (which separate the contribution of different MUs) or blind source separation (BSS) [10] (identifying different muscle contributions by imposing statistical decorrelation or independence) are quite complex and computationally intensive. Thus, they can be impractical in applications (e.g., in contexts like ergonomics [44], sports science [45], gait analysis [46], and clinical settings [47]), where fast setup, recording stability and minimal interference with movement are essential.

In this paper, different methods are proposed to select the weights of a spatio-temporal filter adapting to the recorded signals. HD-EMG with 2-dimensional (2D) grid of electrodes is assumed to be used, but the requirements on the experimental protocol are reduced at a minimum, designing a calibration of the filter on any contraction (better if similar to the one of interest, but without requiring selective activation of single muscles, as for the OSTF [39] or for the NLSTF [40]). Different optimization problems are defined, all promoting sparseness, in order to reduce the effect of crosstalk.

II. METHODS

Let $X \in \mathbb{R}^{N_x \times N_y \times T}$ be the recorded signal from a 2D electrode grid, with spatial dimensions (N_x, N_y) and T time samples. The filter operates over a spatio-temporal window of size $K \times K \times N_t$, where K is an odd spatial kernel size and N_t is the number of taps of a centered temporal filter. At each valid position (i, j) (i.e., for which all electrodes needed for the computation of the filter are available, thus removing locations close to the edges), a spatio-temporal patch is extracted and reshaped into a feature vector $x_{i,j,t} \in \mathbb{R}^{K^2 N_t}$. This vector includes the values from the local spatial neighborhood over N_t time lags:

$$x_{i,j,t} = \mathrm{vec}\left([X(i+u, j+v, t+\tau)]_{u,v,\tau}\right), \tag{1}$$

with $u, v \in [-\lfloor K/2 \rfloor, \lfloor K/2 \rfloor]$ and $\tau \in [-\lfloor N_t/2 \rfloor, \lfloor N_t/2 \rfloor]$.

The filter output is given by:

$$Y(i, j, t) = w^\top x_{i,j,t}, \tag{2}$$

where $w \in \mathbb{R}^{K^2 N_t}$ is the vector of spatio-temporal filter weights to be learned.

The objective is to determine the filter weights w for which the output signals satisfy an optimality criterion. The definition of this criterion enables the formulation of an optimization problem which can be solved for some training data. Then, assuming that the experimental conditions are well represented by the training signals, the estimated filter weights are kept fixed on test data.

In the context of crosstalk, the goal is to discriminate between the signal generated by the target muscle and those originating from nearby. For example, assume that a wearable HD-EMG recording system is placed over an arm or a leg, covering more muscles of interest. In order to correctly characterize the activation of the different muscles, the filter output should be high only when a specific muscle is active. But the diffusion of the potential in the volume conductor makes more channels to register contributions from the same muscles. Thus, to mitigate crosstalk, the desired filter output should compensate for this diffusion of the potential, producing an output which is spatially focused on the channel closest to the source. Building on this idea, different objective functions are presented, defining optimization problems which require the output to be less dispersed across channels. Notice that the proposed approach does not require selective recordings as training data, which could help to discriminate between target and crosstalk signals and were a prerequisite to use other data-driven solutions, like the OSTF [39] and the NLSTF [40].

A. MAXIMUM CORRELATION AND MINIMUM CROSS-CORRELATION

A desired filter output could be that a single channel keeps the signal from near sources, while those same sources remain undetected by the other channels. This way, inter-channel redundancy is reduced and source localization is improved. An objective function keeping this requirement could be one which maximizes the correlation between the filter output $Y(i,j,t)$ and the original signal at the center of the patch, $X(i,j,t)$, while minimizing its correlation with the outputs of the filter from other spatial positions in the array. This approach is conceptually related to the nonlinear Teager-Kaiser energy operator, which subtracts the cross-products of potentials from neighboring electrodes to the squared potential at the detection site, and has been successfully applied to surface EMG spatial filtering in [48]. In contrast, the proposed filter is fully linear, thereby avoiding potential signal distortions introduced by nonlinear operations. Moreover, the filter is trained on signal preliminarily recorded from the subject under study, thus having the possibility to adapt to the specific anatomy and experimental condition. The estimated correlations could be either averaged across channels (inherently assuming that they are positive) or summed after rectification. These two filters are referred to in the following as $Max\bar{C}\&min\bar{X}C$ and $Max|C|\&min|XC|$, respectively.

- In the first case, the following regularized optimization problem is obtained by linearly combining the local correlation, the cross-correlation and a regularization term:

$$\min_w \; -(1-\beta)\mathbb{E}[Y(i,j,t)X(i,j,t)] + \beta\mathbb{E}\left[\sum_{(i',j')\neq(i,j)} Y(i',j',t)Y(i,j,t)^\top\right] + \lambda|w|^2 \tag{3}$$

which can be rewritten as

$$\min_w \; -(1-\beta)\mathbb{E}[x_{i,j,t}X(i,j,t)]^\top w + \beta w^\top \mathbb{E}\left[\sum_{(i',j')\neq(i,j)} x_{i',j',t}x_{i,j,t}^\top\right] w + \lambda|w|^2 \tag{4}$$

where $\mathbb{E}$ averages across channels and time, $\beta \in [0,1]$ is a trade-off parameter that balances signal fidelity and spatial decorrelation, and $\lambda > 0$ is a regularization parameter (chosen by a grid search minimizing the entropy sparsity). Notice that in the expression (4) the filter weights have been taken out and the following terms emerged:

$$\mathbf{r} = \frac{1}{N}\sum_{(i,j,t)} \mathbb{E}\left[x_{i,j,t}X(i,j,t)\right], \tag{5}$$

$$\mathbf{R} = \frac{1}{N(N-1)}\sum_{(i,j)\neq(i',j')} \mathbb{E}_t\left[x_{i,j,t}x_{i',j',t}^\top\right], \tag{6}$$

where $\mathbb{E}_t$ indicates the average over time, N is the number of valid spatial channels and the average over the channels is explicit. Notice that $\mathbf{r}$ is a vector of dimensions $1 \times K^2N_t$ and $\mathbf{R}$ is a matrix $K^2N_t \times K^2N_t$ (where K^2N_t is the number of unknown weights defining the filter vector w). Then, the minimization problem can be written as

$$\min_w \; -(1-\beta)\cdot\mathbf{r}w + \beta\cdot w^\top\mathbf{R}w + \lambda|w|^2 \tag{7}$$

The optimal filter is given by the closed-form solution:

$$w = (\beta\mathbf{R} + \lambda I)^{-1}\cdot(1-\beta)\mathbf{r} \tag{8}$$

which can be implemented efficiently by solving the linear system

$$(\beta\mathbf{R} + \lambda I)\cdot w = (1-\beta)\mathbf{r} \tag{9}$$

- A fully numerical optimization approach was used to manage an objective function considering the sum of rectified cross-correlation terms. In this case, it is simpler to keep the filter w as a tensor with dimensions $K \times K \times N_t$ and compute the output Y by a 3D convolution:

$$Y = X * w, \tag{10}$$

where $*$ denotes the 3D convolution operator and only valid channels are kept. The resulting Y has size $(N_x - K + 1) \times (N_y - K + 1) \times (T - N_t + 1)$.
The filter weights w are learned by optimizing the cost function

$$\mathcal{J}(w) = -(1-\beta)\cdot\mathrm{corr}(Y, X_{\mathrm{center}}) + \beta \cdot \mathrm{ARV}_{i\neq j}\left(\mathrm{corr}(Y_i, Y_j)\right), \tag{11}$$

where corr$(\cdot,\cdot)$ denotes the normalized Pearson correlation, X_{center} is the input channel placed on the center of the filter w, $\text{ARV}_{i\neq j}$ is the sum of the averaged rectified values of the pairwise correlations between different output channels (Y_i and Y_j, with $i \neq j$) and again $\beta \in [0, 1]$ controls the trade-off between fidelity and decorrelation.

The optimization was carried out using a constrained numerical optimizer (i.e., the sequential quadratic programming, SQP). The cost function was evaluated at each iteration by computing the 3D convolution $Y = X * w$, followed by the estimation of the correlation and cross-correlation terms. A nonlinear constraint was enforced in the optimization routine to normalize the weights of the filter to have unity norm. This was accomplished by the function *fmincon* from MATLAB R2025a (fixing the maximum number of iterations to 100 and keeping the other default parameters).

B. MINIMUM ENTROPY

Entropy reaches its maximum for uniformly distributed data and its minimum for sparse values. By enforcing sparsity in the filter output, more spatially focused information can be obtained. As discussed above, this can help reduce crosstalk from nearby muscles and capture localized activity from the detection volume beneath the channel center. However, the resulting waveforms are not expected to resemble those of the raw input data, which may hinder the direct interpretation of the results. This is a key difference with respect to the previous approaches which impose high correlation with the input signal.

The minimization of the entropy of the filter output was obtained on training data using again the function *fmincon* of MATLAB (same parameters as for the $Max|C|\&min|XC|$ filter) with SQP optimizer, imposing the normalization of the weights. This filter is referred to as *MinEntropy* in the following.

C. ADDITIONAL CONSIDERATIONS ON THE FILTERS

1) DIFFERENT OPERATION MODES

Notice that usually the 2D grid is aligned to the muscle fibers, e.g., with the columns of the grid along the fibers' direction and the rows transverse to them. In this condition, crosstalk usually affects the EMG recordings in the direction transverse to that of the muscle fibers, whereas the propagation of the sources along the fibers affects the signals detected along the columns of the grid and the potential should be preserved to avoid distortion. Thus, in this condition, it would be better to reduce the cross-correlation and promote sparseness only in the direction of the rows of the grid. For this reason, three possible modes of spatial decorrelation or sparseness can be implemented:

- *all* – cross-correlation or dispersion are computed across all spatial positions;
- *rows* – only channels on the same row are considered to compute either the cross-correlation or the entropy and then averaged across columns;
- *cols* – only channels on the same column are used to estimate either the cross-correlation or the entropy, averaging then the results across rows.

These modes allow for more structured regularization when spatial dependencies are not isotropic. In the present work, both the configurations *all* and *rows* were applied on simulated signals, obtaining similar results, so that only the former case is discussed.

2) CROSS-VALIDATION FOR PARAMETER SELECTION

The parameters β, K and N_t can be selected through cross-validation. For the specific tests shown below, the only optimized parameter was N_t, which was selected among 1 (only spatial filter) and 3, whereas the other parameters were fixed to $K = 3$ (which allows to have filters centered on the detection point and cover the same region of many popular 2D spatial filters, e.g., the Laplacian) and $\beta = 0.6$ (a sensitivity analysis of this parameter is provided in the Appendix). The number of folds was 5. The cost function for the first two filters based on correlations (i.e., $Max\bar{C}\&min\bar{X}\bar{C}$ and $Max|C|\&min|XC|$) was the ratio of the ARV of the cross-correlations between different output channels and the ARV of the correlations with the input; for the *MinEntropy* filter, the cost was the average entropy of the output. In different applications, performance can be optimize according to a different desired metric (e.g., classification accuracy, source separation quality, maximal cross-correlation in the estimation of conduction velocity, CV).

3) LOCAL AND GLOBAL FILTERS

The filter weights could be obtained either globally (a single shared filter across all spatial positions) or locally (separate filter weights $w_{i,j}$ for each spatial position), the latter leading to increased flexibility and source localization. In this work, however, only global filters have been implemented. This choice has the advantage of leveraging a larger amount of data to estimate the filter weights, leading to a more stable solution. Furthermore, when adjacent channels capture related information (such as delayed contributions caused by action potential propagation along muscle fibers) applying the same weights across locations helps preserve their temporal and spatial correspondence.

4) SYMMETRY

A requirement that can be imposed to the filter is symmetry. Letting the method to select all the weights with minimum constraints (e.g., only normalization) allows to reach a deeper minimum in the cost function, but reducing the degrees of freedom makes the method more stable and less prone to overfitting. For example, by imposing symmetry along both

axes, a 3×3 spatial filter can be written as

$$w = \begin{bmatrix} a & b & a \\ c & d & c \\ a & b & a \end{bmatrix} \quad (12)$$

where a, b, c, and d are the four degrees of freedom (which can be further reduced by additional constraints, such as normalization and zero mean).

Symmetry of the weights was imposed for the two filters requiring numerical optimization (i.e., $Max|C|\&min|XC|$ and *MinEntropy*), not in the case where an analytical solution was available (i.e., $Max\bar{C}\&min\bar{X}C$).

D. TESTING SIGNALS

The method was tested both on simulations and experimental data. Both datasets are described in the following.

1) SIMULATED SIGNALS

The cylindrical model proposed in [49] was used to simulate monopolar single fiber action potentials (SFAP) from a grid of 5×11 electrodes with 5 mm of inter-electrode distance (IED), covering two adjacent muscles. The properties of the volume conductor and the location of fiber sources are represented in Figure 1A-C and the location of the electrode grid in Figure 1D. Notice that three volume conductors have been considered, with fat layer thickness of 3 mm, 7 mm or 12 mm, respectively. Fibers were simulated with density of 20 fibers/mm^2, approximately the MU fiber density and one order of magnitude lower than the muscle fiber density [50]. The number of fibers per MU followed an exponential distribution in the range 15-300.

A total of 200 MUs were simulated. Ten different libraries of MUAPs were built, assigning randomly the size of the MUs. MU locations were uniformly distributed across the muscle cross-section, and the fibers closest to each MU center were assigned to it. The corresponding SFAPs were summed to generate the MUAP (introducing a small error, as the SFAPs of the same fibers could be included in different simulated MUAPs). MU CV followed a Gaussian distribution (mean 4 m/s, SD 0.3 m/s), with values assigned according to the size principle [51].

The control of MUs was described as in [52], considering the distributions of recruitment thresholds and firing rates (FR) of the vastus lateralis muscle, but rescaling to get minimum and maximum FR equal to 5 and 35 Hz, respectively. The ISI was assumed to have a Gaussian distribution with coefficients of variation equal to 10%. Force levels varying over time were simulated, as shown in the Results section.

White Gaussian noise with SNR 30 dB or 20 dB was finally added to the simulated monopolar signals.

2) EXPERIMENTAL SIGNALS

The experimental dataset is the same as in [40] and [53] (to which the reader can refer for details). In short, eight healthy subjects were recruited. Monopolar EMGs were recorded using an electrode grid of 13×5 with IED of 8 mm during contractions of flexor carpi radialis (FCR) and pronator teres (PT). Surface EMGs were amplified, band-pass filtered (−3 dB bandwidth, 10-500 Hz), sampled at 2048 Hz and converted in digital form with a resolution of 16-bit (Quattrocento, OT Bioelettronica, Turin, Italy). Ideally, two columns were over the FCR, two on the PT and the central one in between.

The contractions were quite selective, as the subjects were asked to make either a flexion or a pronation. The applied force was recorded by load cells and a visual feedback was provided to the subject to ask to produce a constant level: 10%, 20%, 40% and 50% MVC were successfully recorded from all subjects and used for testing. The recorded signals had duration of 10 s. A portion 5×5 of the grid showing the largest EMG amplitude during the recordings was considered. A small portion of the data was used for training: non-selective contractions were simulated by summing the signals recorded at 20% MVC of the FCR muscle with those at 40% MVC of the PT muscle, and vice versa (40% MVC FCR + 20% MVC PT). The resulting signals were then concatenated. For testing, the central epochs of 8 s were selected from each recording and concatenated to simulate alternating selective contractions.

The experiments were conducted in accordance with the Declaration of Helsinki and with the approval of the Ethical Committee of University of Turin (approval number 510190).

E. TEST OF PERFORMANCES

Before filtering, the signals were extended by symmetry on the borders: if along a direction we have N electrodes indicated with the numbers $1, \cdots, N$, the virtual electrodes 0 and $N + 1$ were added with the same signals as for electrodes number 2 and $N - 1$, respectively. As $K = 3$, this choice allowed to get the same space dimension for the raw and filtered signals, simplifying the comparisons. The same approach was implemented a long time, in the case in which $N_t = 3$.

Different performance indicators were considered: the signal-to-crosstalk ratio (SCR) and the correlation coefficient (CC) of envelopes of the actual and crosstalk-free signals recorded from channels over a specific muscle. Moreover, two dispersion indexes were monitored: the cross-correlation and the entropy dispersion. Statistical analysis was performed to compare the performance across four filters: raw monopolar signals, $Max\bar{C}\&min\bar{X}C$, $Max|C|\&min|XC|$ and *MinEntropy*.

In estimating the envelope, the electrodes over each muscle were considered separately (i.e., the 5 columns over each muscle, for simulations; column 2 and 4 for FCR and PT, respectively, in the experimental data); selective activations of the muscle under the electrodes were used for the reference signal; average envelopes were then estimated for the two muscles and used to compute the CC, comparing the reference with the output of each filter.

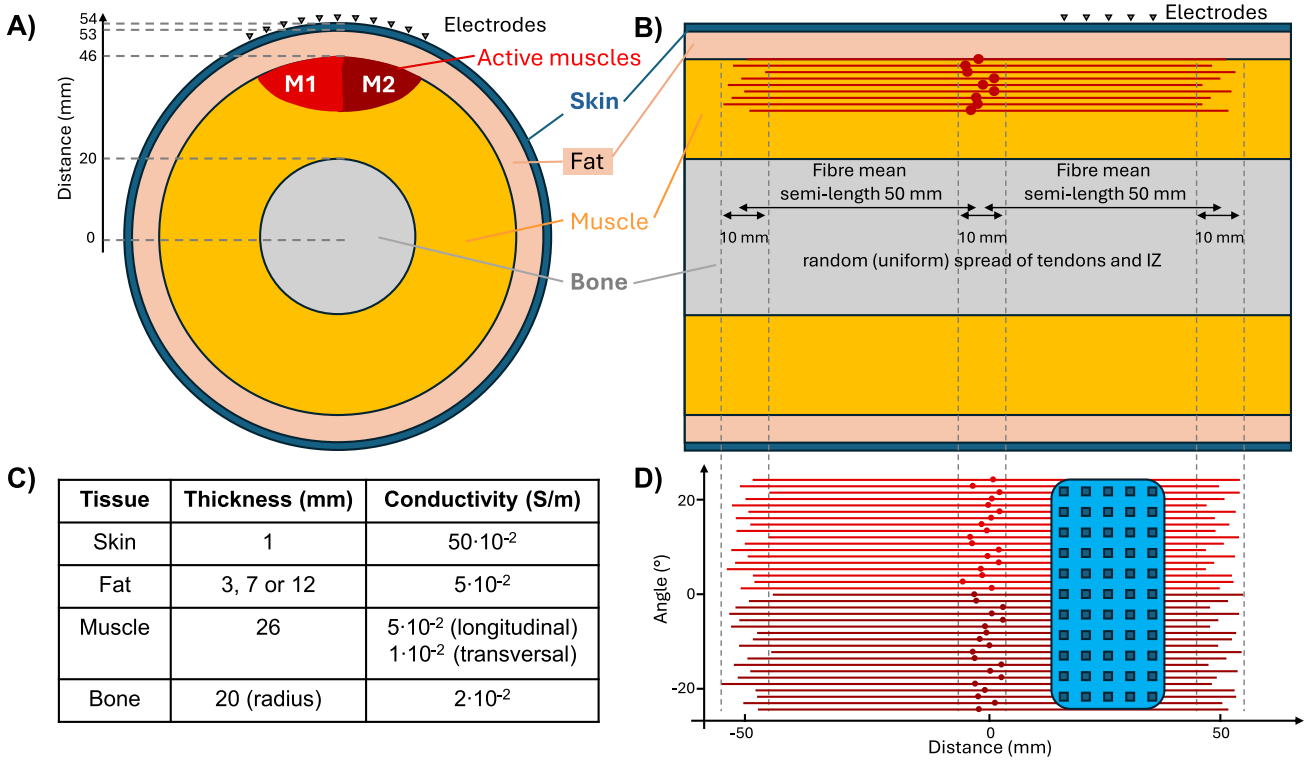

Tissue	Thickness (mm)	Conductivity (S/m)
Skin	1	$50{\cdot}10^{-2}$
Fat	3, 7 or 12	$5{\cdot}10^{-2}$
Muscle	26	$5{\cdot}10^{-2}$ (longitudinal) $1{\cdot}10^{-2}$ (transversal)
Bone	20 (radius)	$2{\cdot}10^{-2}$

FIGURE 1. Description of the simulation model. A) Cross-section of the volume conductor, with indication of the thickness of the layers (case of 7 mm of fat thickness), of the active muscles and of the electrodes. B) Longitudinal section of the volume conductor, with indication of the mean fibers lengths, spread of the tendons and innervation zone (IZ). C) Parameters of the tissues. D) Top view of the simulated model, with indication of the 2D grid of electrodes and relative location of the fibers of the simulated active muscles.

All analyzes were performed using MATLAB R2025a. Different analyzes were applied to the results of tests on simulated and experimental data, as detailed below.

1) SIMULATED DATA PROCESSING

For each performance or dispersion index, a linear mixed-effects (LME) model was applied to evaluate the impact of the filter, subcutaneous fat thickness, and SNR on the metric. The LME framework allows to account for the correlation between repeated measurements on the same simulated signals.

Let y_{ijkm} denote the observed value of the metric for the i-th signal, fat level j, SNR level k, and processing method m (i.e., the filter used). The model is specified as

$$y_{ijkm} = \mu + \text{Method}_m + \text{Fat}_j + \text{SNR}_k + b_i + \varepsilon_{ijkm} \quad (13)$$

where

- μ is the overall intercept,
- Method_m is the fixed effect of the m-th signal processing method ($m = 1, \ldots, 4$),
- Fat_j is the fixed effect of the j-th fat thickness level,
- SNR_k is the fixed effect of the k-th SNR level,
- $b_i \sim \mathcal{N}(0, \sigma_b^2)$ is the random intercept representing the i-th signal, capturing within-signal correlations across methods,
- $\varepsilon_{ijkm} \sim \mathcal{N}(0, \sigma^2)$ is the residual error term.

By including the signal as a random effect, the model accounts for the repeated-measures nature of the data, since each simulated signal is processed by all methods. Pairwise comparisons between methods were performed using contrasts on the estimated fixed effects. Possible significant differences between each filter and raw data were indicated. Statistical significance was assessed at $\alpha = 0.05$. Residual normality was assessed with the Lilliefors test; data were log-transformed when necessary.

2) EXPERIMENTAL DATA PROCESSING

Due to the small size of the experimental dataset ($n = 8$), non-parametric statistics was applied. Possible statistically significant differences between raw and filtered data were tested for each performance metric using the Wilcoxon signed rank method. Significance was assessed at $\alpha = 0.05$.

III. RESULTS

Figure 1 shows the simulation model used to generate HD-EMGs under controlled conditions. Specifically, Figure 1A and 1B show cross-sectional and longitudinal views of the volume conductor, respectively, illustrating the different tissue layers, the geometry of muscle fibers, the distribution of IZs and tendon endings, and electrode placement. The model parameters are summarized in Figure 1C

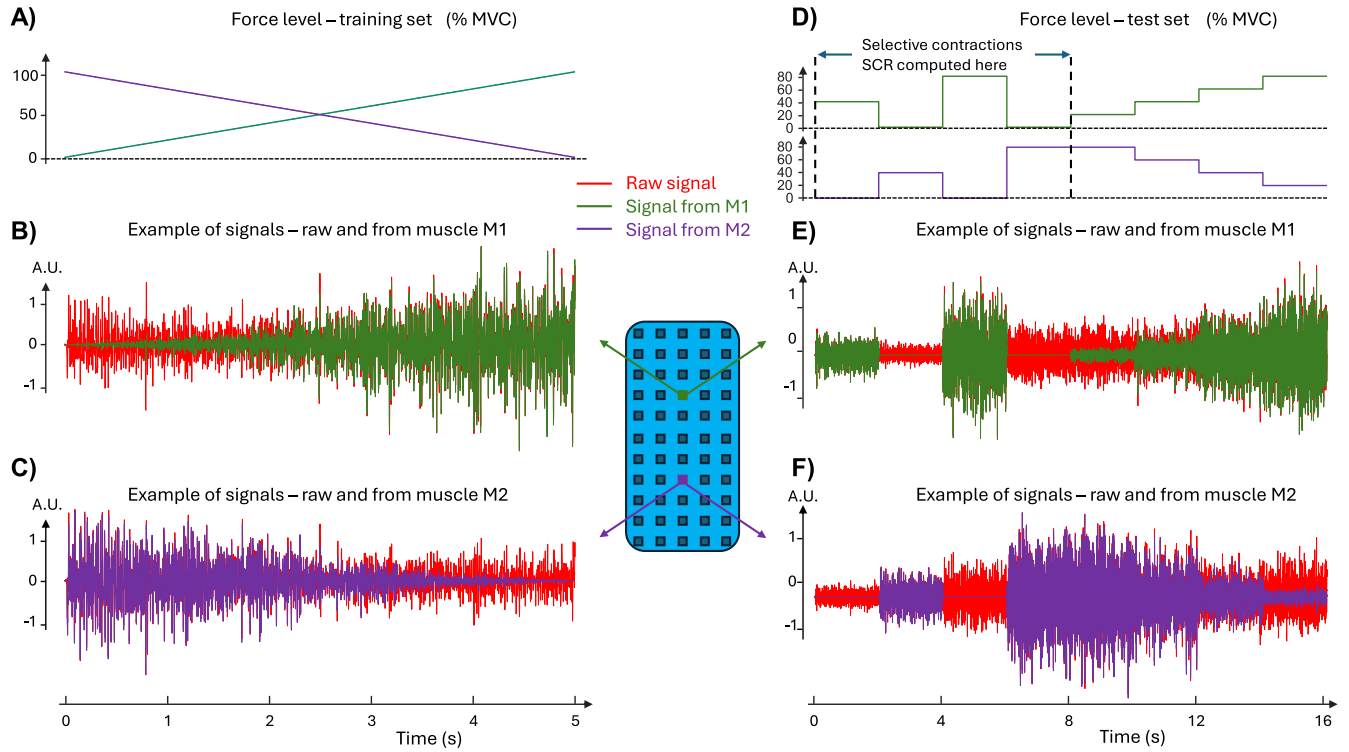

FIGURE 2. A) Simulated force levels of the two muscles (green and violet for the first and second muscle, respectively) for training the filters (volume conductor with fat thickness of 7 mm, additive noise with SNR of 30 dB). B) Example of signal from an electrode placed over the first muscle (M1): both the training signal (red) and the one produced by M1 (green) are shown. C) Example of signal from an electrode placed over the second muscle (M2): both the training signal (red) and the one produced by M2 (violet) are shown. D) Simulated force levels of the two muscles for testing the filters. The first portion shows selective contractions, from which the signal-to-crosstalk ratio (SCR) is computed. E) Example of signal from an electrode placed over M1: both the test signal (red) and the one produced by M1 (green) are shown. F) Example of signal from an electrode placed over M2: both the test signal (red) and the one produced by M2 (violet) are shown.

and Figure 1D provides a top view of the electrode grid and the spatial distribution of the simulated active muscle fibers.

Figure 2 presents the simulated force levels and an example of the corresponding signals recorded at some individual electrodes over both muscles. Figure 2A illustrates the training signals: notice that the contractions of the two muscles were not selective, but they were co-contracted with an opposite force level linearly varying in time. Panels B and C show the signals measured at electrodes over the muscles, indicated as M1 and M2, respectively, highlighting the contribution of each muscle to the recorded signals. Panels D-F illustrate the signals during test contractions, including selective contractions used to compute the SCR and another portion with a co-contraction of the two muscles with different time dynamics.

Preliminary examples of the application of different filters to the test data are shown in Figure 3. Panels A, B and C show the filters $Max|C|\&min|XC|$, *MinEntropy* and $Max\bar{C}\&min\bar{X}\bar{C}$, respectively, applied to the test data shown in Figure 2. Panels D-G display the envelope of the raw and of the processed signals across the electrode grid, averaged along the fiber direction. The results highlight differences in the spatial and temporal distribution of the processed signals depending on the filter used. All the 3 proposed filters reduce the dispersion of the potential and provide a better estimate of the true envelope.

Figure 4 illustrates the effect of the filters on SFAPs generated by fibers at different depths within the muscle (1 mm and 8 mm). The filters are the same discussed in the previous Figure, trained on interference raw signals generated with the same volume conductor model used to simulate the SFAPs. Panels A-B show the raw potential distributions over the skin, while Panels C-D, E-F, and G-H display the SFAPs after processing by the three different filters: $Max|C|\&min|XC|$, *MinEntropy* and $Max\bar{C}\&min\bar{X}\bar{C}$, respectively. The filters affect both the amplitude and spatial distribution of the SFAPs, with deeper fibers showing a larger dispersion across the electrode grid. The dispersion of the SFAPs is largely reduced by the filters with respect to the raw data. The EMG amplitude is reduced when comparing the superficial and deep fiber, with the raw signal showing a reduction factor of about 12, whereas the filters are more selective, but still preserve substantial residual potential from the deep fiber (with reductions of about 18 to 30).

Figures 5 and 6 show the overall results obtained by processing the simulation dataset. Notice that the dataset includes 60 simulations, i.e., 10 subjects $\times$ 3 fat layer thicknesses $\times$ 2 SNRs of the additive noise. The type of processing

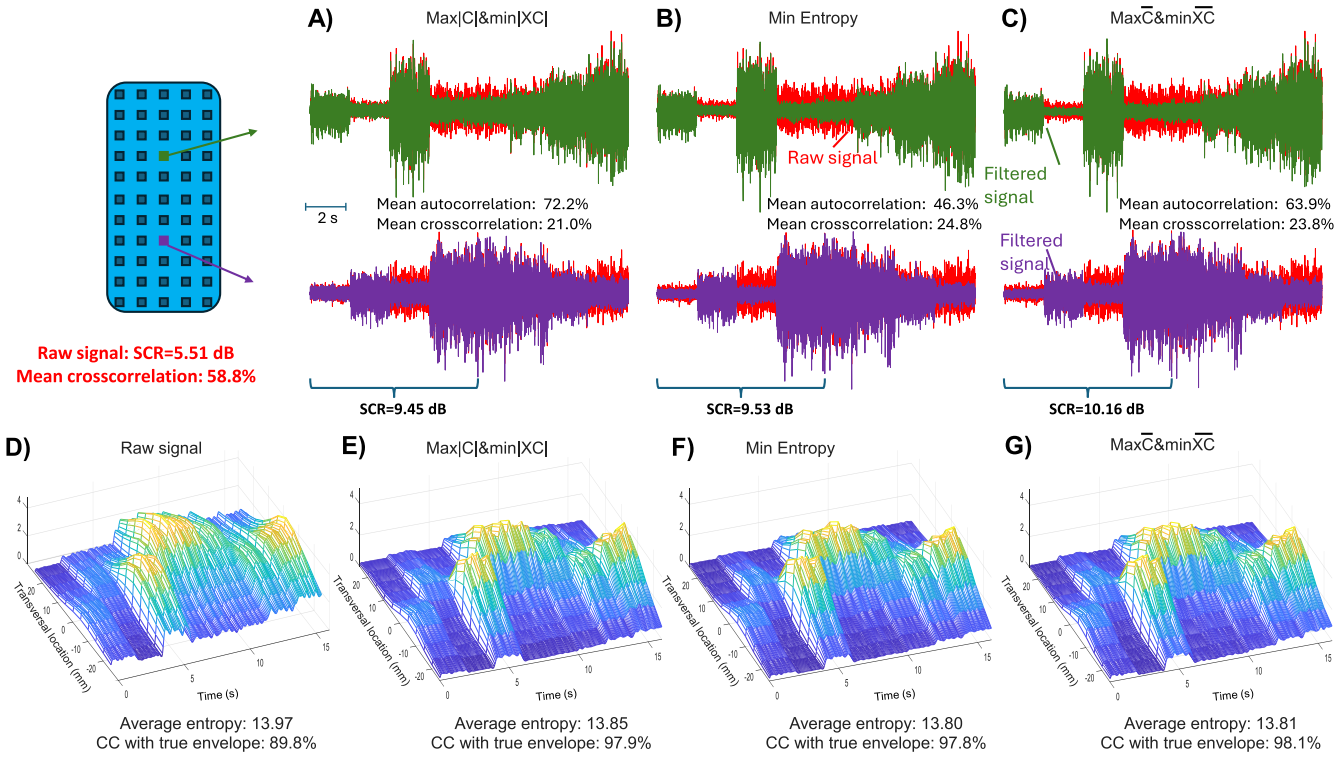

FIGURE 3. Example of application on test data (same data as in Figure 2). A) Application of the filter which maximizes the modulus of the correlation with the input and minimizes the modulus of the cross-correlation of the output. B) Application of the filter which minimizes the entropy of the output. C) Application of the filter which maximizes the mean of the correlation with the input and minimizes the mean of the cross-correlation of the output. D) Envelope (absolute value of the signal low-pass filtered at 4 Hz) of the raw signal, averaged across the 5 electrode arrays along the fibers direction, shown as a function of the transverse location of the electrodes and time (down-sampled of a factor 100). E) Average envelope for the signals processed by the filter in A). F) Average envelope for the signals processed by the filter in B). G) Average envelope for the signals processed by the filter in C).

selected by cross-validation of the training data was a simple spatial filter in 32, 2, and 56 cases (out of 60 simulations), for $Max|C|\&min|XC|$, *MinEntropy* and $MaxC\&minXC$, respectively. Another general result is the local correlation between the raw and filtered signals: in terms of mean±std, it is 74.6±5.3, 31.3±34.2 and 72.0±10.2, for $Max|C|\&min|XC|$, *MinEntropy* and $MaxC\&minXC$, respectively (showing a low correlation for the *MinEntropy*, which is not designed to keep the correlation with the raw data).

Figure 5 summarizes the performance of the different filtering methods in reducing crosstalk between muscles. The upper panels show the pooled results across all simulated conditions, whereas the middle and lower panels illustrate the outcomes obtained when data are grouped according to fat layer thickness and noise levels, respectively. For all metrics, significant differences were observed between the raw and the processed signals obtained using any of the filters ($p < 0.001$). Panel A reports the average SCR computed across all 25 detection channels over each muscle (thus removing the central array of electrodes, placed between the two muscles). All the proposed filters substantially increased the SCR compared to the raw data, indicating a reduced contribution of signals originating from adjacent muscles. No significant effect was disclosed for the factors fat and SNR. However, a clear inverse trend is noticed between SCR and fat layer thickness, which is aligned to expectations, as a thicker fat increases the effect of crosstalk [31]. Panel B shows the correlation coefficient (CC) between the average envelopes of the correct and estimated signals (where the signals considered to be correct are those from the muscle below the electrodes, not perturbed by the crosstalk contribution from the other). The CC values confirm the improved selectivity of the filtered signals, with only minor differences between the filters under the same conditions. Also in this case, neither fat nor SNR had a significant effect, with the factor fat being close to significance (indicating that it is easier to estimate the envelope when the fat is thinner, as the detection is more selective in that case).

Figure 6 presents the results for the spatial dispersion metrics of the potentials detected over the skin. As in the previous figure, data are shown both pooled across conditions and separated according to fat thickness and noise level. Panel A illustrates the average cross-correlation across channels, which quantifies the spatial overlap of the detected signals. The filters markedly reduced this value relative to the raw signals, reflecting a more localized spatial distribution of the MUAPs after processing. No statistically significant effects were observed for either fat or SNR (however, an increasing trend of cross-correlation with fat layer thickness is observed,

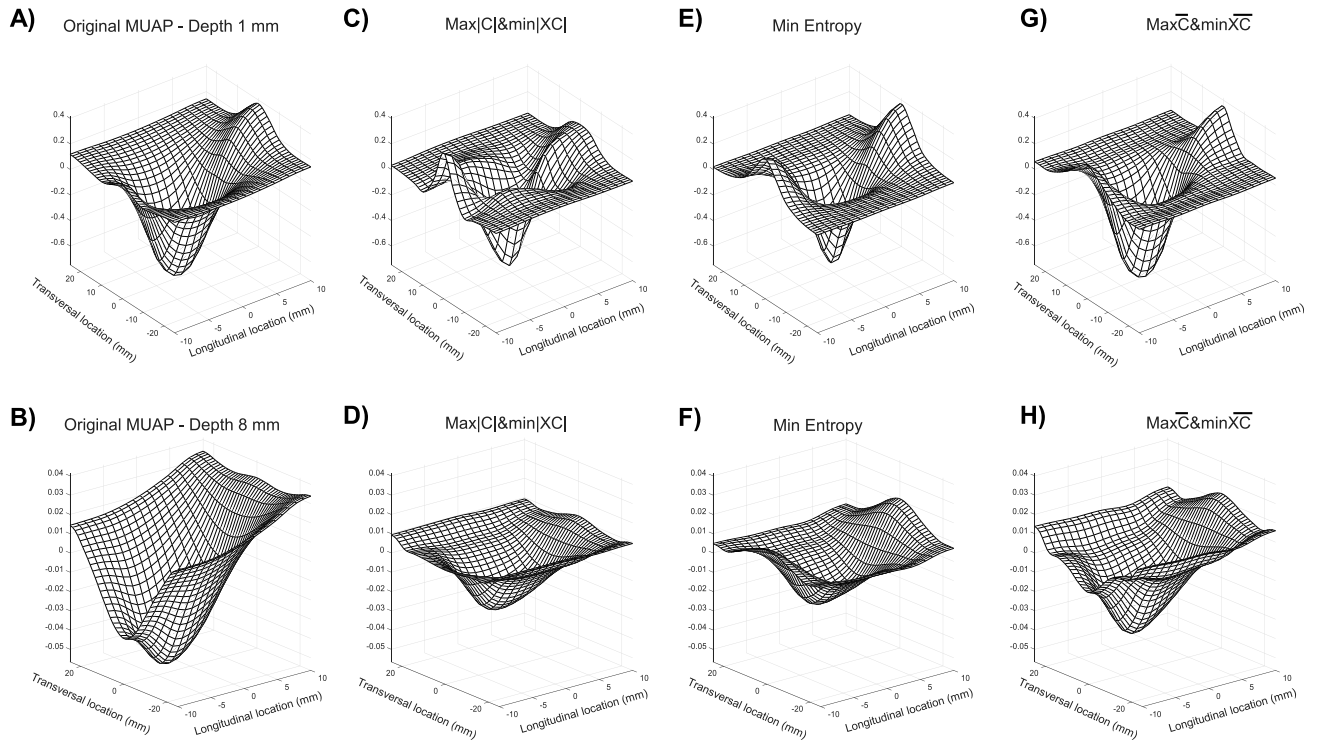

FIGURE 4. Effect of the different filters on SFAPs from fibers placed under the center of the electrode grid and of different depths (1 mm and 8 mm within the muscle; same volume conductor and filters as in the previous Figure). The potentials are normalized with respect to the range of the A)-B) Distribution of the potentials over the skin (oversampling by a factor 4 the detection by the electrode grid, for representation purposes) in a specific time sample, for the fibers with the two depths, respectively. C)-D) Same SFAPs as in A)-B) obtained after processing by the filter which maximizes the modulus of the correlation with the input and minimizes the modulus of the crosscorrelation of the output. E)-F) Same SFAPs as in A)-B) obtained after processing by the filter which minimizes the entropy of the output. E)-F) Same SFAPs as in A)-B) obtained after processing by the filter which maximizes the mean of the correlation with the input and minimizes the mean of the crosscorrelation of the output.

as it emphasizes the effect of crosstalk). Panel B shows the average entropy of the detected potentials, as a measure of the spatial spreading of the signal over the skin. The lower entropy values obtained after filtering indicate a more focused potential distribution, confirming that all tested filters effectively enhanced spatial selectivity. No significant effects were found for the factors fat and SNR, with the factor fat being close to significance (with smaller entropy for thinner fat layers, as the potential is less dispersed in such a case).

Figure 7 shows the results of the tests on the experimental data. The training data were very short: 625 ms, in which a small portion of the signals from flexion and pronation were summed and concatenated. Notice that the dataset includes 8 subjects. The type of processing selected by cross-validation of the training data was a simple spatial filter in 1, 1, and 5 cases (out of 8), for the $Max|C|\&min|XC|$, *MinEntropy* and $Max\bar{C}\&min\bar{XC}$, respectively. The dispersion of the signal was significantly reduced by all the methods, as indicated by a smaller cross-correlation between channels and entropy with respect to the input data. The performances in reducing crosstalk indicate median improvements for all filters with respect to the raw data, reflected by a larger SCR (median paired improvement of 0.67, 1.61 and 1.01 dB for $Max|C|\&min|XC|$, *MinEntropy* and $Max\bar{C}\&min\bar{XC}$, respectively) and CC of the envelope of the single muscle (improvement of 2.4, 2.5, 3.1 %, respectively), but only a few cases are significant: the increase of SCR for the *MinEntropy* filter and the improved envelope estimation for the $Max\bar{C}\&min\bar{XC}$ filter.

The local correlation between the raw and filtered signals, in terms of mean±std, is 69.0±4.2, 20.6±16.6 and 38.1±33.7, for $Max|C|\&min|XC|$, *MinEntropy* and $Max\bar{C}\&min\bar{XC}$, respectively.

Notice that the tests in simulation and experiments were done in very different conditions, e.g., in terms of electrode density (55 and 25 electrodes with IED of 5 mm and 8 mm for simulations and experiments, respectively), type of activations and duration of the training signals (5 s and 0.625 s, respectively), in addition to the deviations from ideal conditions in the real data (e.g., misalignment with respect to the electrode grid, small muscle shifts and fiber rotations during the contractions, more muscles than expected contributing to the signal). The influence of specific parameters and the extraction of additional information is investigated in the Appendix for a few cases. Specifically, a default simulation model was considered: fat thickness of 7 mm, noise level with SNR of 30 dB, electrode grid with 55 electrodes and IED of 5 mm. Then, the following conditions were tested:

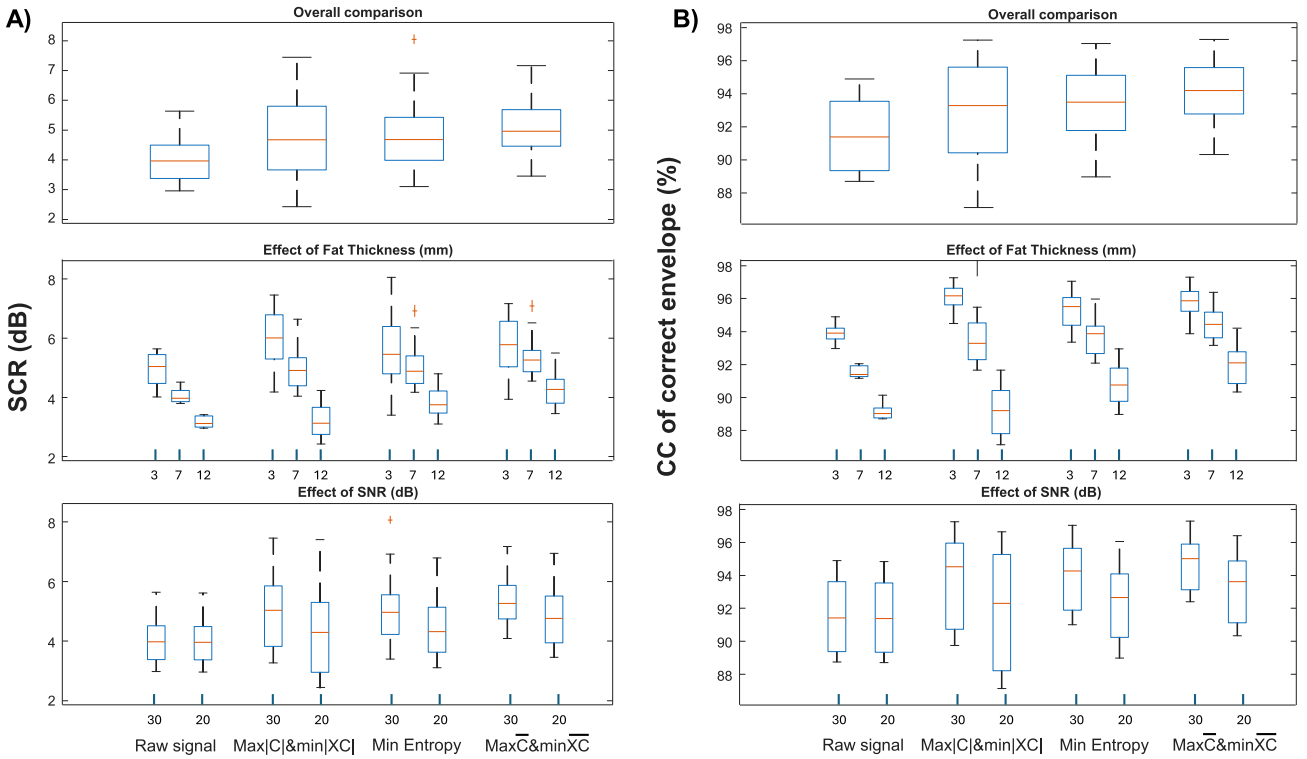

FIGURE 5. Simulation dataset: general performance in crosstalk reduction. Comparison of different filtering methods, either pooling all data (top), or splitting different fat layer thicknesses (middle) or noise levels (down). Box and whisker plots are shown, indicating median, quartiles and range. Significant pairwise comparisons between raw signals and all filters ($p<0.001$). No significant effect of fat and SNR. A) Average signal-to-crosstalk ratio (SCR) estimated considering all 25 channels over each muscle. B) Correlation coefficient (CC) of the average envelopes: correct versus estimated.

- variation of the tradeoff parameter β on $Max|C|\&\ min|XC|$ filter;
- removal of symmetry constraint on the filter *MinEntropy*;
- different values of IEDs, duration of the training signal, rotation of the electrode grid with respect to the muscle fibers, estimation of CV and median frequency (MDF) using $Max\bar{C}\&min\bar{X}\bar{C}$ filter.

These tests are only a few of the possible of interest and should be considered only preliminary, but all confirm that reducing the dispersion of the electric potential by the proposed filters improves the performance on information extraction (EMG amplitude, CV, MDF from the target muscle) with respect to using the raw data.

IV. DISCUSSION

The present study proposes different filtering strategies for reducing crosstalk in surface EMG recordings and evaluates their performance through both a simulation framework and experimental tests. The common thread among all proposed methods is that they are data-driven: the filter weights are not pre-determined (as in classical spatial filters), but are instead obtained by optimizing problem-specific cost functions.

In addition, the proposed filters can operate on samples acquired at nearby time instants as well as at neighboring electrode locations, thus defining spatio-temporal filters that provide greater flexibility than traditional purely spatial approaches. The filter weights are chosen so as to reduce the dispersion of the outputs, thereby yielding signals that are more spatially focused on the underlying bioelectric sources. This makes the filters ideally dependent only on the recording conditions (i.e., on the volume conductor, location of electrodes, muscles under investigation) and not on the specific signals used to calibrate them. This is a further distinguishing feature of the proposed approach with respect to other existing methods that require dedicated training data obtained from specific motor tasks (e.g., selective contractions).

A. GENERAL CONSIDERATIONS ON SPATIAL FILTERS

Spatial filters are typically designed to accomplish a specific task, such as increasing spatial selectivity [48] (e.g., to improve EMG decomposition), removing some signal components (e.g., end-of-fiber effects [2], [12]), improving the estimation of physiological parameters (e.g., muscle fiber CV [54]), or enhancing the target muscle activity with respect to crosstalk [39]. When applied to HD-EMG recordings obtained with a regular grid of electrodes, these filters operate according to the same rule at each spatial location, effectively performing a spatial convolution, similarly to filtering masks in image processing. This inherently assumes that the volume conductor is space invariant [55] and the electrode grid well

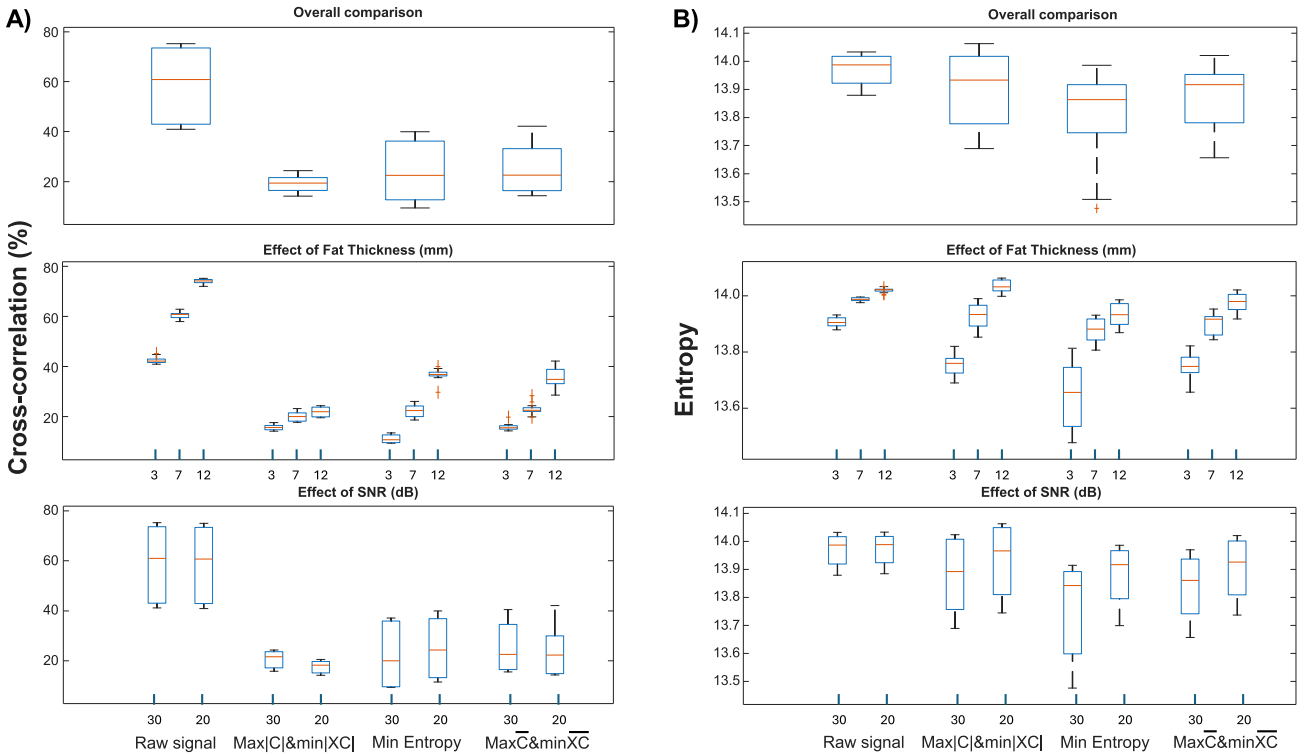

FIGURE 6. Simulation dataset: metrics of dispersion of the potential over the skin. Comparison of different filtering methods, either pooling all data (top), or splitting different fat layer thicknesses (middle) or noise levels (down). Box and whisker plots are shown, indicating median, quartiles and range. Significant pairwise comparisons between raw signals and all filters ($p<0.001$). No significant effect of fat and SNR. A) Average cross-correlation across channels. B) Average entropy.

aligned to the muscle fibers, which in turn should be parallel to each other.

In order to achieve their objective, spatial filters search from neighboring electrodes the information needed to generate their output. Notice that if we were to evaluate the quality of a filter solely based on the reduced dispersion of the potential and consequential increase of sharpness of the MUAPs, a trivial approach (that would not even require information from neighboring electrodes) would be to elevate the signal of each individual channel to a power larger than 1. This improved localization could be measured by indexes like entropy or kurtosis (which are respectively smaller and larger in the presence of highly peaked waveforms). For instance, the signal detected over the FCR shown in Figure 7B exhibits entropy and kurtosis equal to 11.0 and 21.0, respectively. Using the output of the *MinEntropy* filter shown in Figure 7C, the dispersion is reduced, obtaining entropy and kurtosis equal to 10.9 and 50.8, respectively. However, if we compute them after elevating the signal to the power 3, they are 8.4 and 1497.4, showing a smaller dispersion; if we elevate it to a larger power (e.g., 11, which is again an odd number, to keep the sign) the dispersion is getting still smaller (entropy 3.4 and kurtosis 18642.0). Nevertheless, this trivial way of reducing dispersion does not reflect any deterministic property of surface EMG and therefore lack physiological interpretability. Moreover, the reduced dispersion of the time series obtained by raising the values to a large exponent is nonlinear (thus, not satisfying the superposition principle) and does not provide additional informative value to the recorded signal (which could instead be gained by incorporating information from other sampled locations); rather, it merely produces a sparser signal by amplifying outliers (e.g., MUAPs from large MUs located close to the electrodes) while attenuating smaller contributions (e.g., MUAPs from small or deep sources), which may nonetheless be relevant, as they could originate from the target muscle. For instance, considering deeper fibers producing a surface potential which is 10 times smaller than superficial fibers (i.e., a similar situation as in Figure 4), by elevating the signal to the power m we would get an amplitude which is 10^m times smaller.

The use of a spatial filter is a more reasonable approach, which is grounded in the biophysics underlying surface EMG generation. In fact, EMG reflects the diffusion of the electric potential within the volume conductor, governed by quasi-electrostatic principles [13]. Specifically, the EMG results from the solution of Poisson equation, which relates the bioelectric sources (namely the transmembrane currents flowing across the sarcolemma) to the potential diffusing in the volume conductor. In principle, the EMG could be found by inverting the Laplacian operator and applying it to the bioelectric current sources. This observation could

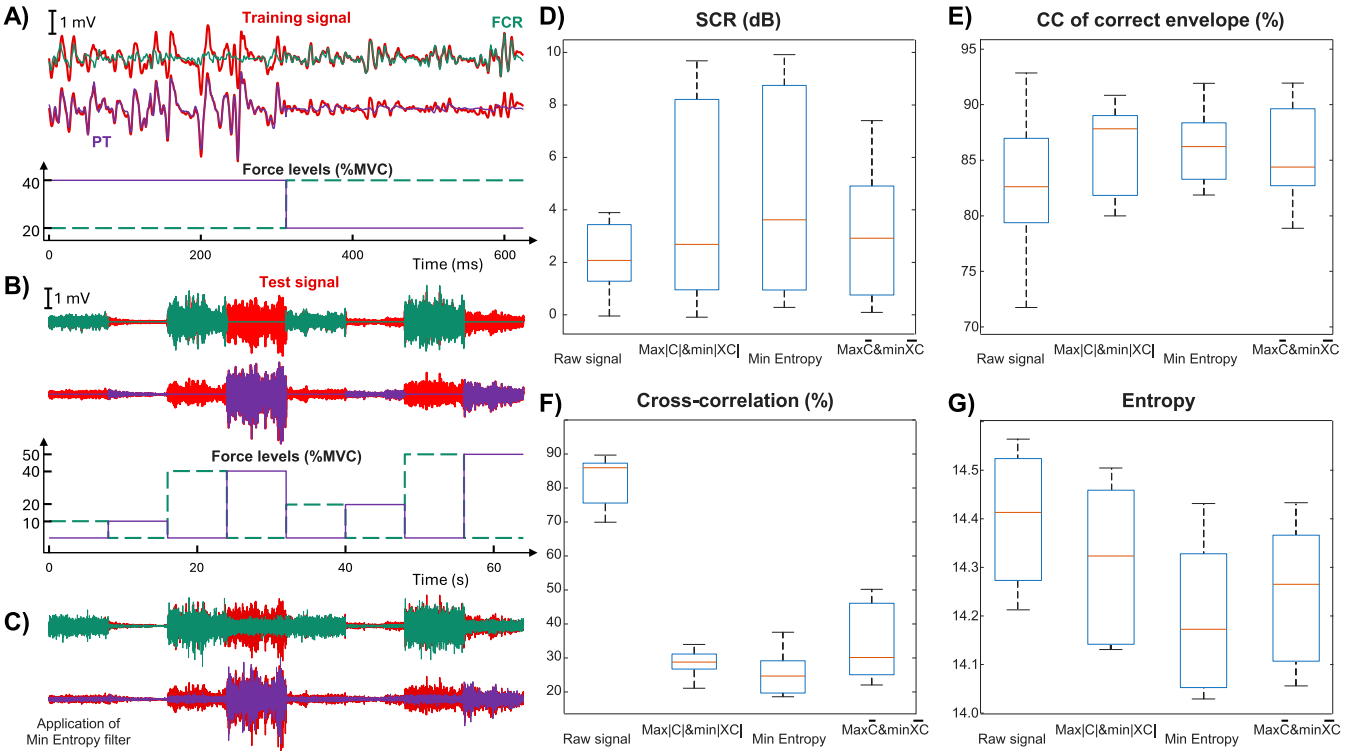

FIGURE 7. Experimental dataset: performance in reducing the effect of crosstalk and the dispersion of the potential over the skin. Comparison of different filtering methods. A) Example of training data, recorded from the central electrodes of the second and fourth columns (expected to be over the muscles Flexor Carpi Radialis and Pronator Teres, FCR and PT, respectively), with indication of the exerted force levels of the signals that were summed and concatenated. Here and in B and C, the processed data is in red, whereas green and violet colours refer to FCR and PT, respectively. B) Test signal (from the same electrodes as in A), composed of the concatenation of 8-s epochs of selective contractions of different force levels (indicated down). C) Test data as in B, with the filtered signal superimposed (*MinEntropy* filter was considered). D) Box and whisker plots (indicating median, quartiles and range) of the signal-to-crosstalk ratio (SCR) for the raw signal and the different filters, considering the 5 channels of the columns 2 and 4 (for FCR and PT, respectively). Significant pairwise comparisons between raw signals and *Min Entropy* filter ($p<0.05$). E) Correlation coefficient (CC) of the average envelopes of the correct and estimated signal from the muscles under the detection points (second and fourth columns for FCR and PT, respectively). Significant pairwise comparisons between raw signals and *MaxC̄&minX̄C̄* filter ($p<0.05$). F) Average cross-correlation across channels. Significant pairwise comparisons between raw signals and all filters ($p<0.01$). G) Average entropy. Significant pairwise comparisons between raw signals and all filters ($p<0.01$).

provide a key for understanding the rationale behind the use of a Laplacian filter, which, when applied to the EMG, makes an inverse operation with respect to the solution of the forward Poisson problem (giving the potential induced by the current sources) to provide focused information on the bioelectric sources. Similar interpretations could be given to other pre-defined filters (e.g., single and double differential) which have a high-pass behaviour in the spatial frequency domain, which in part can compensate the low-pass effect of the volume conductor.

In practice, however, the volume conductor has complicated conductivity (as tissues are inhomogeneous and anisotropic) and geometry [13], which makes the simple pre-defined filters not optimal. In this regard, the information from nearby electrodes becomes crucial to explore the dispersion of the surface potential in order to design strategies to compensate for it. If detailed knowledge on the volume conductor is available, a filter inverting its low-pass filtering effect could be designed (as shown in [56] for a plane layer volume conductor model). As an alternative, a data-driven approach can be used to obtain directly the weights of the filter by processing some preliminary data. The effectiveness of data-driven strategies has been demonstrated in several applications, including the discrimination of the contribution of different muscles with BSS [10], the crosstalk reduction using the OSTF [39] and the estimation of the bipolar signal from noisy recordings with the NLSTF [40].

In the present study, the same underlying principle is exploited to reduce the spatial dispersion of the EMG potential over the skin surface by jointly considering spatial and temporal information (i.e., potentials from neighboring electrodes and consecutive time samples), thereby providing great flexibility in achieving the desired output. The results indicate that this approach leads to measurable improvements in crosstalk reduction, while also highlighting some limitations that warrant further investigation in future studies, as discussed in the following sections.

B. DISCUSSION OF THE RESULTS

The results demonstrated that all the proposed filters substantially improved the selectivity of the detected signals by reducing their spatial dispersion over the skin and by increasing the SCR. These effects were consistent across different levels of simulated subcutaneous fat thickness

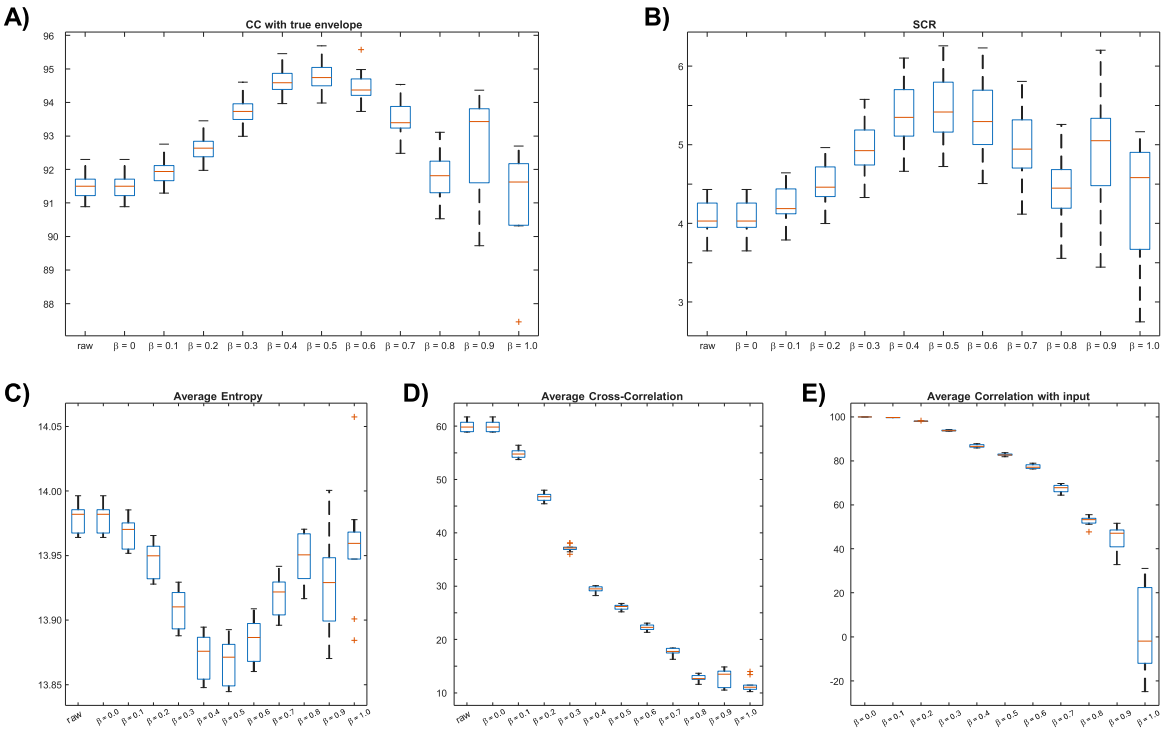

FIGURE 8. Test on *Max|C|&min|XC|* of the effect of the parameter β, weighting the correlation with the input and the cross-correlation between output channels on the optimized functional: $\mathcal{J}(w) = -(1-\beta)\cdot \text{corr}(Y, X_{\text{center}}) + \beta \cdot \text{ARV}_{i\neq j}\left(\text{corr}(Y_i, Y_j)\right)$. The same simulated data configuration as in Figure 5 were used, considering a fat layer thickness of 7 mm and noise with SNR = 30 dB. A) Correlation coefficient (CC) with the envelope of the crosstalk-free simulated signal. B) Signal-to-crosstalk ratio (SCR). C) Average entropy of the signal, as a measure of dispersion. D) Average cross-correlation of output channels, as another measure of dispersion of the surface potential. E) Correlation between raw and filtered data.

and noise, indicating that the filters are robust under various physiological and recording conditions. Specifically, Figures 3 and 4 show preliminary qualitative indications that the proposed filters indeed reduce the dispersion of the potential (both in interference signals and single SFAPs), allowing to decrease the effect of crosstalk. Then, Figures 5 and 6 demonstrate on the entire simulated dataset that the proposed filtering strategies significantly improve the discrimination of muscle activity by simultaneously reducing crosstalk and increasing the spatial focus of the detected potentials across a wide range of tissue and noise conditions.

The reduction in signal dispersion observed after filtering suggests that the processed EMG signals become more spatially confined to the active muscle region. This result is particularly relevant for applications in which selective detection of muscle activity is required, such as MU decomposition, neuromuscular modelling, and the control of myoelectric interfaces. By attenuating the contribution of nearby muscles, the filters improve the correspondence between the electrical activity detected on the skin and the underlying muscle sources.

The simulation approach used in this work made it possible to systematically investigate the influence of tissue properties and noise on the performance of each filter. The results confirmed that crosstalk contamination increases with thicker subcutaneous fat layers, due to the enhanced spatial blurring of the volume conductor. Nevertheless, all filters tested were able to significantly mitigate this effect, supporting their potential use in realistic recording conditions. In addition, the robustness of the filters to different noise levels suggests their applicability in experimental and clinical contexts where signal quality may vary.

All the evaluated methods (i.e., filters based on correlation or entropy optimization) showed similar overall performance (with some problems observed for the *Max|C|&min|XC|* filter, with 12 mm of fat layer thickness), indicating that multiple cost functions can effectively exploit the spatio-temporal structure of EMG signals to enhance selectivity. The improvement in both target signal recovering (in terms of SCR and envelope estimation) and spatial localization metrics (cross-correlation and entropy) highlights the consistency between the different measures of filter performance.

The crosstalk reduction achieved by the filters was also observed in experimental data (Figure 7), although the small dataset and the imperfectly selective contractions limited the statistical significance.

Simulation and experimental tests span a broad range of conditions, as details on signal generation (ideal vs. real volume conductor), recording (different density and distribution of the electrodes) and filter training (activation of

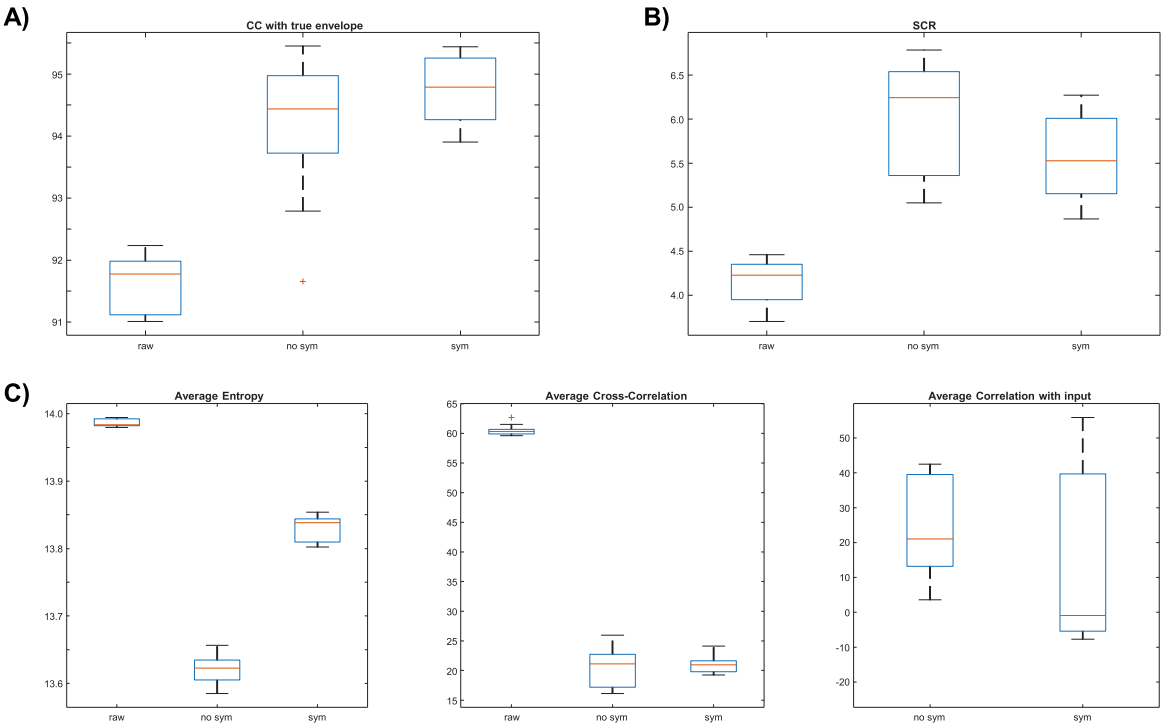

FIGURE 9. Test of the symmetry constraint on the filter *MinEntropy*. The same simulated data configuration as in Figure 5 were used, considering a fat layer thickness of 7 mm and noise with SNR = 30 dB. The symmetry constraint was either imposed (sym) or not (no sym). A) Correlation coefficient (CC) with the envelope of the crosstalk-free simulated signal. B) Signal-to-crosstalk ratio (SCR). C) Average entropy of the signal, as a measure of dispersion. D) Average cross-correlation of output channels, as another measure of dispersion of the surface potential. E) Correlation between raw and filtered data. All paired comparisons of raw and each of the filtered data are statistically significant (Wilcoxon signed-rank test).

the muscles and duration of training phase) differed significantly. However, additional ablation and sensitivity tests are collected in the Appendix, focusing on individual deviations from a default simulation model. All tests confirmed the importance of reducing signal dispersion and the value of the proposed filters.

C. LIMITATIONS AND FUTURE WORKS

The innovative filters were applied to signals heavily affected by crosstalk, acquired using monopolar detection with a small IED and with two muscles in close proximity. As any filtering operation inevitably introduces signal distortion, a careful evaluation of its benefits and drawbacks is therefore warranted before data processing. In the specific conditions investigated here, there was substantial room for improvement and the underlying assumptions of the methods were reasonably satisfied. In other general applications, the user should consider that the proposed filters linearly combine potentials from neighboring electrodes and from consecutive time samples; thus, a clear rationale is required to justify that the integrated information is indeed beneficial for achieving the intended goal (namely, crosstalk reduction in this study). For instance, electrodes should be sufficiently close to capture contributions from common sources; otherwise, their combination may be of limited relevance. In summary, while the effectiveness of the proposed filters has been demonstrated under the tested conditions, their generalization to different recording setups should be carefully evaluated.

Another critical point to be acknowledged is that the present work is primarily based on simulated EMG data, with only a preliminary experimental validation. The simulation framework incorporates realistic anatomical and electrophysiological parameters and allows performance evaluation under controlled conditions, where a precise reference is available. Moreover, the simulation dataset was large and specific details (fat layer thickness, noise, random distribution of the MUs in the muscles) have been integrated separately, to explore their effect. This represents a key advantage for the systematic assessment of the proposed filtering approach.

Nonetheless, an extended experimental validation will be required to fully confirm the observed improvements under real recording conditions, where several confounding factors may affect the performances. The relatively large variability observed in the limited experimental dataset highlights the intrinsic challenges associated with real EMGs.

In particular, the experimental analysis relied on the assumption that the recordings were performed under selective activation conditions, such that the signal detected over the relaxed muscle could be attributed mainly to crosstalk. However, visual inspection suggests that a residual activity of the muscle assumed to be relaxed was likely

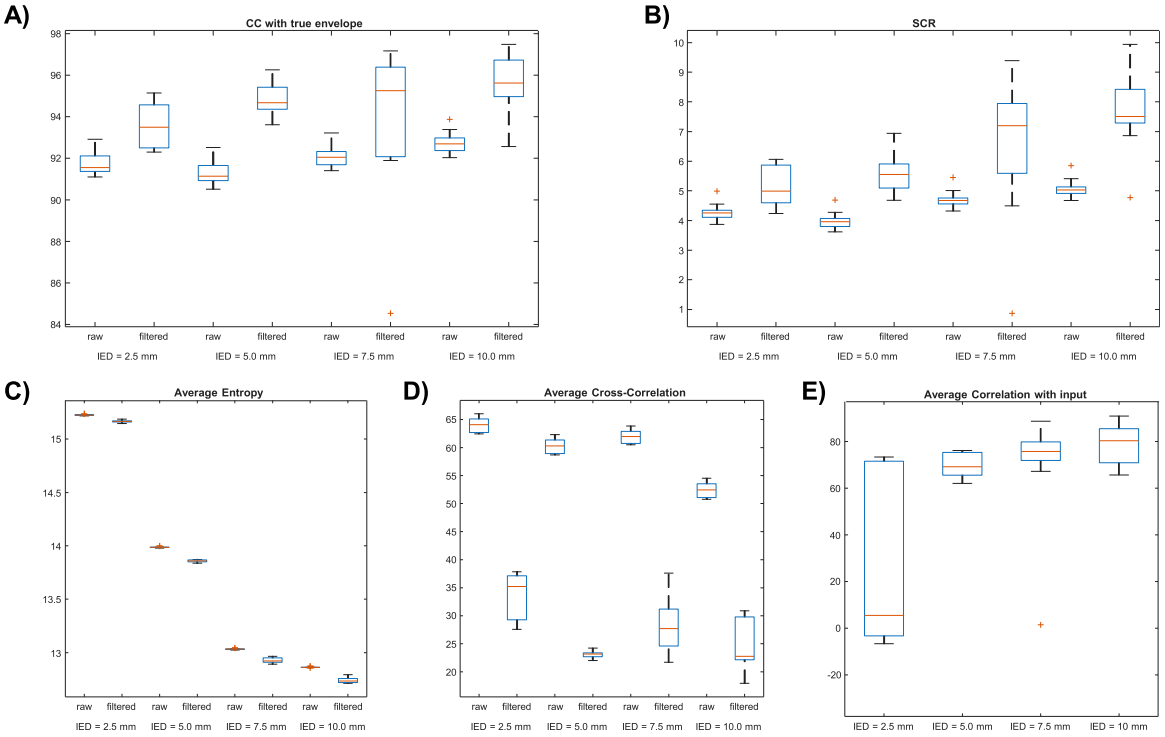

FIGURE 10. Test on $Max\overline{C}\&min\overline{XC}$ of the effect of changing the inter-electrode distance (IED) of the simulated data. The same volume conductor and configuration as in Figure 5 were used, considering a fat layer thickness of 7 mm and noise with SNR = 30 dB. A very dense electrode grid with IED of 2.5 mm was simulated: then, electrodes were down-sampled, taking 1 over 2, 3, and 4 to get IED equal to 5 mm (same as the default tests), 7.5 mm and 10 mm, respectively. A) Correlation coefficient (CC) with the envelope of the crosstalk-free simulated signal. B) Signal-to-crosstalk ratio (SCR). C) Average entropy of the signal, as a measure of dispersion. D) Average cross-correlation of output channels, as another measure of dispersion of the surface potential. E) Correlation between raw and filtered data. All reported results show statistically significant differences between raw and filtered data under same conditions (Wilcoxon signed-rank test), with the exception of the CC and SCR metrics at an inter-electrode distance of 7.5 mm.

present. Moreover, only two muscles (FCR and PT) were considered as contributors to the recorded EMG, whereas additional neighboring muscles may also have influenced the measurements. For example, Figure 7C reveals an unexpected reduction of EMG amplitude recorded over the PT muscle when comparing the 40% and 50% MVC force levels; this raises the suspicion that a change in selectivity or an additional contribution from other muscles may have occurred.

Furthermore, as mentioned above, the proposed spatial filtering approach implicitly assumes a space-invariant volume conductor, enabling the use of a fixed global filter (which is applied as a spatial convolution over the surface EMG map). On the other hand, local variations in geometry and tissue conductivity are expected. In addition, small muscle displacements may occur across different contractions, violating the ideal assumption of constant relative positions between sources and detection points. These factors may limit the direct transferability of the simulation-based results to experimental scenarios.

Thus, further applications on real data is fundamental, and future work is suggested to extend the proposed approach, assessing whether the same filters (or others obtained by a data-driven optimization of alternative cost functions) can consistently and robustly enhance signal selectivity. Moreover, it would be important to verify their stability in dynamic conditions or in the presence of geometrical deformations. The value of the proposed approach in experimental tests could also be assessed on the basis of the possible improved outcomes in specific applications, for example the followings.

1) Decomposition of the interference signal into single MUAP trains. Reducing the spread of the surface potential could help separating different contributions from single MUs.
2) Optimization of myoelectric control by processing data focused on the muscles under the detection point.
3) Estimation of muscle synergies, based on data less affected by crosstalk.
4) Estimation of activation intervals (e.g., in gait analysis).
5) Basic physiology studies (e.g., on myoelectric manifestations of fatigue), in which the focus on specific target sources (single MUs or muscles) is important.

V. CONCLUSION

A filter inevitably alters the input signal, emphasizing certain information over others. Therefore, it is not meaningful to claim that a filter is optimal unless it is tailored to a specific

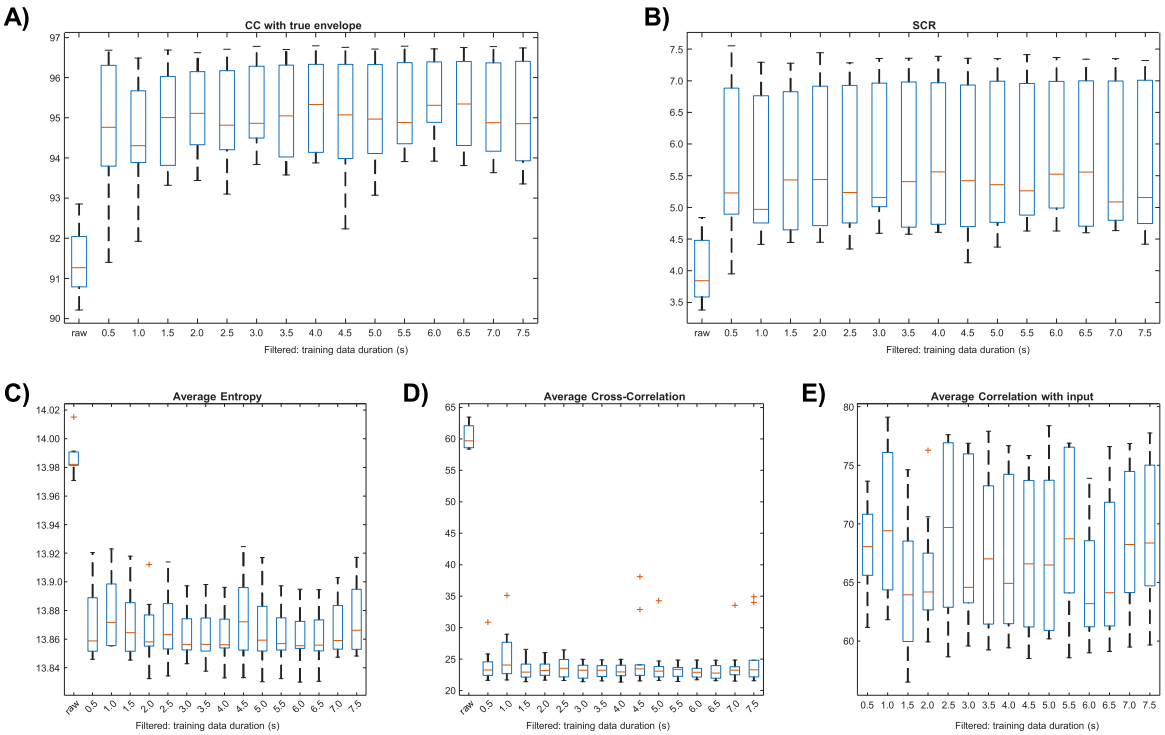

FIGURE 11. Test on $Max\overline{C}\&min\overline{XC}$ of the effect of changing the duration of the training data. The same configuration as in Figure 5 was used, considering a fat layer thickness of 7 mm and noise with SNR = 30 dB. The training data was the EMG corresponding to the sum of two force ramps, as in Figure 2A, but with different durations. A) Correlation coefficient (CC) with the envelope of the crosstalk-free simulated signal. B) Signal-to-crosstalk ratio (SCR). C) Average entropy of the signal, as a measure of dispersion. D) Average cross-correlation of output channels, as another measure of dispersion of the surface potential. E) Correlation between raw and filtered data.

application. Moreover, it would be wise to design a filter considering the desired output information to be extracted.

This work proposes a data-driven approach for the definition of spatio-temporal filters for pre-processing HD-EMGs. A cost function is defined to measure the electric potential dispersion across different electrodes and filter weights are chosen to minimize it. This allows to get more selective information (either promoting output fidelity with the input signal or not, as for the correlation and entropy based costs, respectively). The filters are trained on some preliminary recordings before being applied on new data; however, no specific calibration requirements are imposed beyond asking the subject to contract all muscles of interest (e.g., separate selective contractions for each muscle are not required). Thus, in practical implementations, the operator could optimize the filter on data recorded during a short preliminary contraction in which more muscles are activated and then the experiment can start, using the pre-processing online.

This form of personalization aligns with recent perspectives on hyper-personalized medicine within the Healthcare 5.0 paradigm, which emphasizes tailoring data processing pipelines to individual physiological and anatomical characteristics rather than relying solely on population-level models [58]. In this context, subject-specific adaptation of the spatial filter for EMG pre-processing represents a consistent strategy to improve robustness and interpretability in real-world signal analysis.

Based on simulation and experimental tests, this study demonstrates that the proposed data-driven filtering can effectively reduce crosstalk and improve the spatial selectivity of surface EMGs, with promising potential for practical applications.

Crosstalk was here chosen as prototype problem, but other applications, e.g., robust CV estimation, could be investigated with a similar approach.

APPENDIX
ADDITIONAL SIMULATION RESULTS

Additional tests on sensitivity to parameters and ablation studies are shown here. Tests on single filters have been performed, considering a default simulation model, with average thickness of the fat layer, a small amount of additive noise and the same electrode grid shown in Figure 1. Ten subjects were simulated for each explored condition.

A test on the computational costs of the training phase has been performed. The algorithms were implemented in MATLAB R2025a and computations were performed on a fixed workstation featuring an AMD Ryzen 7 9700X CPU (8 physical cores, 16 logical threads, 3.8 GHz) and 64 GB of RAM. A dedicated GPU was not used. The times for training on 5 s simulated signals (including the selection

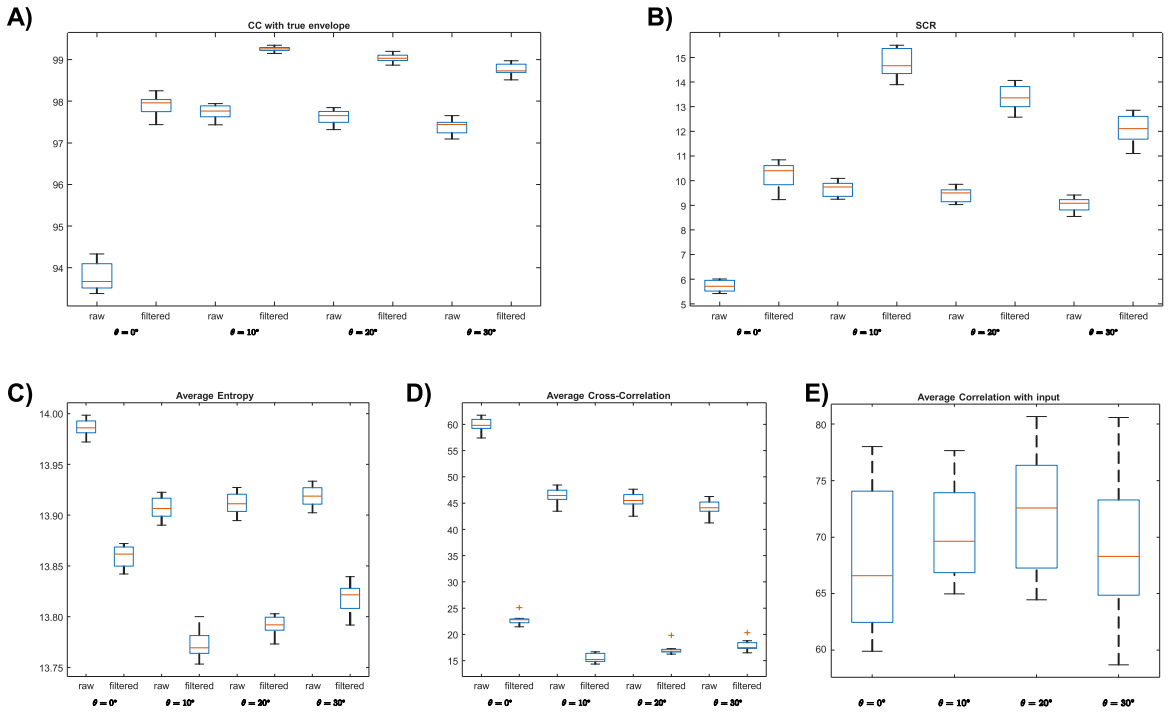

FIGURE 12. Test on $Max\bar{C}\&min\overline{XC}$ of the effect of rotating the electrode grid, producing a misalignment with respect to the muscle fibers. The same configuration as in Figure 5 was used, considering a fat layer thickness of 7 mm and noise with SNR = 30 dB, but the recording grid was rigidly rotated around its center of an angle $\theta \in [0^o, 30^o]$. Different performance and dispersion indexes are computed on both the raw and filtered signals. The channels considered covering the first muscle included the electrode grid columns from 1 to 5, those from 7 to 11 were over the second muscle (excluding the column number 6 allowed to keep all electrodes over the correct muscle also with the largest considered rotation). A) Correlation coefficient (CC) with the envelope of the crosstalk-free simulated signal. B) Signal-to-crosstalk ratio (SCR). C) Average entropy of the signal, as a measure of dispersion. D) Average cross-correlation of output channels, as another measure of dispersion of the surface potential. E) Correlation between raw and filtered data. All reported results show statistically significant differences between raw and filtered data under same conditions (Wilcoxon signed-rank test).

of the optimal parameters by cross-validation) for the filters $Max|C|\&min|XC|$, *MinEntropy* and $Max\bar{C}\&min\bar{X}\bar{C}$ were 139.49±7.40 s, 114.16±13.16 s and 2.21±0.14 s, respectively (given as mean ± standard deviation).

Figure 8 illustrates the effect of the parameter β, which balances the correlation with the input signal and the cross-correlation among output channels in the optimized functional (given in Equation (11)). The tests were performed for the filter $Max|C|\&min|XC|$. The analysis shows how varying β influences both performance (in terms of the CC with the envelope of the crosstalk-free reference and the SCR) and dispersion-related metrics (including entropy and inter-channel correlation). The results highlight the trade-off between preserving the desired signal content and reducing inter-channel redundancy. Specifically, small values of β prioritize fitting the input signal (with $\beta = 0$ yielding an output identical to the input), whereas larger values increasingly emphasize cross-correlation reduction and lower signal dispersion, with values around $\beta = 0.5$ also leading to minimum entropy dispersion.

The same tests were also applied to the filter $Max\bar{C}\&minX\bar{C}$, but the results were very stable (except for the case $\beta = 0$), as the regularization parameter λ of Equation (3) (selected to minimize entropy dispersion) compensates in part for the variation of β.

Figure 9 reports the impact of imposing a symmetry constraint on the *MinEntropy* filter. In the average, the envelope of the crosstalk-free signal is estimated better and the SCR is improved less when using the symmetric constraint (Figure 9A and 9B, respectively), indicating that there is not a clearly better solution for the specific test signals. Smaller electric potential dispersion is achieved when removing the symmetry constraint (Figure 9C and 9D), as it allows the filter to better adapt to the data (due to the additional degrees of freedom). The match with the processed signal is not imposed, and this is reflected with a small correlation with the input (Figure 9F).

The influence of the IED is analyzed in Figure 10. Starting from a very dense simulated grid, different IEDs were obtained through spatial down-sampling. The figure shows how increasing electrode spacing affects the ability of the method to suppress crosstalk while preserving signal quality, as reflected by the considered performance and dispersion measures. In general, the observed dispersion is lower when the IED is larger. However, the filtered signal shows always improved performances and reduced dispersion with respect to the raw data.

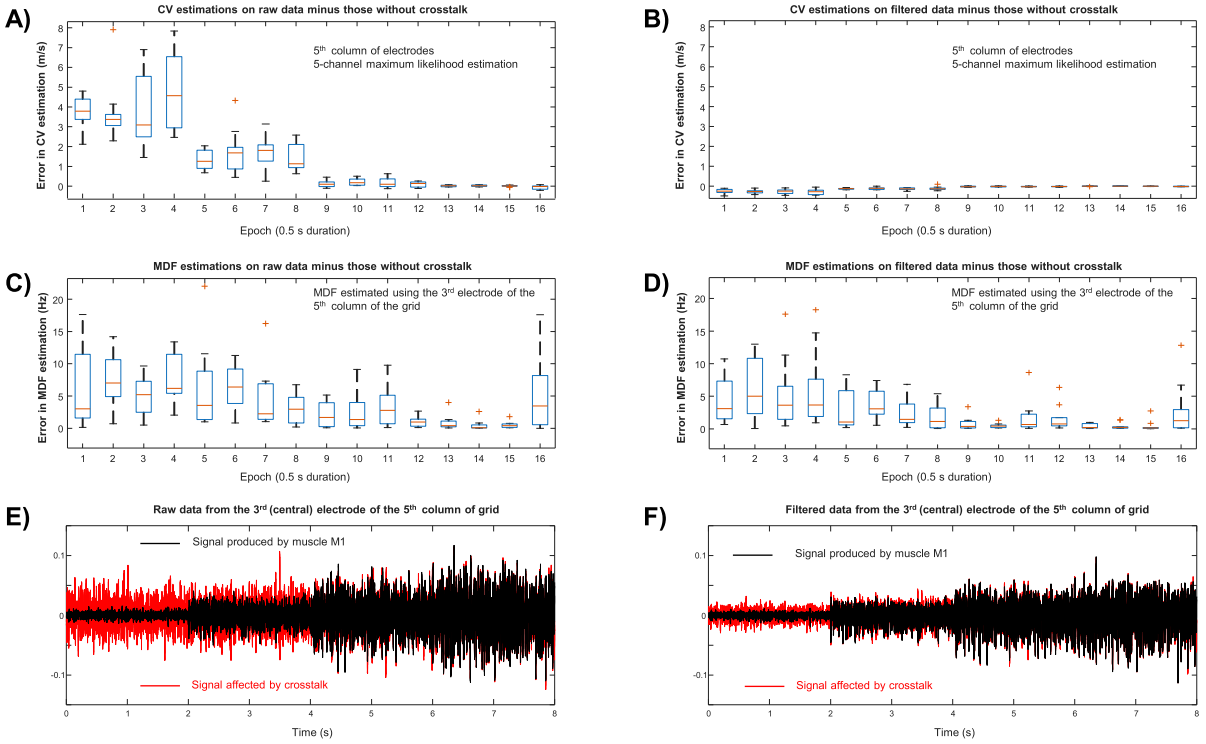

FIGURE 13. Error in the estimation of EMG indexes. The filter $Max\bar{C}\&min\overline{XC}$ is used, applied on data simulated with the same configuration as in Figure 5, with a fat layer thickness of 7 mm and noise with SNR = 30 dB. The last 8 s of test signal were used (both muscles are activated, M1 with 4 steps of increasing force levels, M2 with an opposite pattern). Data were segmented into 16 adjacent and non-overlapping epochs of 0.5 s. Conduction velocity (CV) was estimated by a multi-channel maximum likelihood method [57]. The muscle M1 was considered and the fifth column of electrodes was used (i.e., the closest to the crosstalk muscle). A) Difference between the estimation of CV using the raw data or the crosstalk-free signals. Mean absolute error = 1.45 m/s. B) Difference between the estimation of CV using the filtered data or the filtered crosstalk-free signals. Mean absolute error = 0.11 m/s (statistically smaller than for raw data, according to the Wilcoxon signed rank test). C) Difference between the median frequency (MDF) estimated using the raw data from the third electrode and the corresponding crosstalk-free signal. Mean absolute error = 3.95 Hz. D) Difference between the MDF estimated using the filtered data from the third electrode and the filtered crosstalk-free signal. Mean absolute error = 2.55 Hz (not statistically lower than for the raw data). E) Example of raw data from one of the ten simulated subjects: comparison of processed data and crosstalk-free (i.e., M2 switched off). F) Same signals as in E), but processed by the filter.

Notice that, for the smallest IED considered, the correlation with the input exhibits large variability and a low median. This arises because enforcing a low cross-correlation between potentials recorded by very close electrodes degrades the fidelity of the filtered signal with respect to the input. This issue is mitigated when using the *rows* modality (i.e., reducing cross-correlation only between channels in the transverse direction, and not along the muscle fiber direction; see Section II-C1); for larger IEDs, this filter yields results comparable to those observed in the figure.

Figure 11 investigates the effect of the duration of the training data on filter performance. Different training lengths were considered using the same simulated configuration. The filter appears to provide fairly stable results even with short training data.

The robustness of the proposed method to electrode grid misalignment with respect to muscle fiber orientation is assessed in Figure 12. By progressively rotating the recording grid around its center, the analysis evaluates the effect of spatial misalignment on both raw and filtered signals. Performance is not degraded by this specific test. Across all considered rotation angles, the filtered data consistently exhibit statistically significant improvements with respect to the input signals.

It is worth noting that the $Max\bar{C}\&min\bar{X}\bar{C}$ filter is not constrained to be symmetric. This property is expected to be advantageous in the presence of geometric perturbations with respect to the ideal configuration, as electrode misalignment with muscle fibers would otherwise make symmetry constraints potentially detrimental by forcing equality among non-equivalent electrodes. To further investigate this aspect, the same test was repeated using the *MinEntropy* filter with an imposed symmetry constraint: results indicate that *MinEntropy* and $Max\bar{C}\&min\bar{X}\bar{C}$ filters have similar performances, thus suggesting that the symmetry constraint does not degrade substantially the performance of the filter up to 30^o of misalignment.

Finally, Figure 13 quantifies the error in the estimation of relevant EMG indexes. The comparison between raw and filtered signals demonstrates a substantial reduction in CV estimation error due to crosstalk after filtering and moderate improvements for MDF estimation. Nevertheless,

these results should be interpreted with caution. When global indexes are extracted from interference EMGs, the contributions of different sources are combined through a complex weighted averaging process [35], which depends on the detection volume of the employed filter. In this study, the estimates obtained from crosstalk-free signals (either raw or filtered) were used as reference values to specifically assess the perturbing effect of crosstalk. However, in practical applications, it is crucial not only to mitigate crosstalk (e.g., by reducing the detection volume), but also to ensure that the extracted index remains representative of the activity of the target muscle, which may be compromised if the detection volume becomes excessively small [38], [39], [40]. Further investigation is thus recommended to improve the estimation of meaningful EMG indexes from crosstalk-affected data, depending on the specific application of interest.

ACKNOWLEDGMENT

Experimental data were recorded by Dr. M. Raggi under the supervision of Prof. G. Boccia of the NeuroMuscularFunction Research Group, Department of Clinical and Biological Sciences, University of Torino, Turin, Italy.

REFERENCES

[1] G. R. Naik, D. K. Kumar, and M. Palaniswami, "Signal processing evaluation of myoelectric sensor placement in low-level gestures: Sensitivity analysis using independent component analysis," *Expert Syst.*, vol. 31, no. 1, pp. 91–99, Feb. 2014.

[2] L. Mesin, S. Smith, S. Hugo, S. Viljoen, and T. Hanekom, "Effect of spatial filtering on crosstalk reduction in surface EMG recordings," *Med. Eng. Phys.*, vol. 31, no. 3, pp. 374–383, Apr. 2009.

[3] N. S. Stoykov, M. M. Lowery, and T. A. Kuiken, "A finite-element analysis of the effect of muscle insulation and shielding on the surface EMG signal," *IEEE Trans. Biomed. Eng.*, vol. 52, no. 1, pp. 117–121, Jan. 2005.

[4] L. Mesin, "Simulation of surface EMG signals for a multilayer volume conductor with a superficial bone or blood vessel," *IEEE Trans. Biomed. Eng.*, vol. 55, no. 6, pp. 1647–1657, Jun. 2008.

[5] M. M. Lowery, N. S. Stoykov, A. Taflove, and T. A. Kuiken, "A multiple-layer finite-element model of the surface EMG signal," *IEEE Trans. Biomed. Eng.*, vol. 49, no. 5, pp. 446–454, May 2002.

[6] M. M. Lowery, N. S. Stoykov, J. P. A. Dewald, and T. A. Kuiken, "Volume conduction in an anatomically based surface EMG model," *IEEE Trans. Biomed. Eng.*, vol. 51, no. 12, pp. 2138–2147, Dec. 2004.

[7] C. J. De Luca, M. Kuznetsov, L. D. Gilmore, and S. H. Roy, "Inter-electrode spacing of surface EMG sensors: Reduction of crosstalk contamination during voluntary contractions," *J. Biomechanics*, vol. 45, no. 3, pp. 555–561, Feb. 2012.

[8] D. Farina, R. Merletti, B. Indino, M. Nazzaro, and M. Pozzo, "Surface EMG crosstalk between knee extensor muscles: Experimental and model results," *Muscle Nerve*, vol. 26, no. 5, pp. 681–695, Nov. 2002.

[9] D. Farina, L. Arendt-Nielsen, R. Merletti, B. Indino, and T. Graven-Nielsen, "Selectivity of spatial filters for surface EMG detection from the tibialis anterior muscle," *IEEE Trans. Biomed. Eng.*, vol. 50, no. 3, pp. 354–364, Mar. 2003.

[10] D. Farina, C. Fevotte, C. Doncarli, and R. Merletti, "Blind separation of linear instantaneous mixtures of nonstationary surface myoelectric signals," *IEEE Trans. Biomed. Eng.*, vol. 51, no. 9, pp. 1555–1567, Sep. 2004.

[11] R. Merletti, C. J. De Luca, and D. Sathyan, "Electrically evoked myoelectric signals in back muscles: Effect of side dominance," *J. Appl. Physiol.*, vol. 77, no. 5, pp. 2104–2114, Nov. 1994.

[12] D. Farina, L. Mesin, S. Martina, and R. Merletti, "Comparison of spatial filter selectivity in surface myoelectric signal detection: Influence of the volume conductor model," *Med. Biol. Eng. Comput.*, vol. 42, no. 1, pp. 114–120, Jan. 2004.

[13] L. Mesin, "Volume conductor models in surface electromyography: Computational techniques," *Comput. Biol. Med.*, vol. 43, no. 7, pp. 942–952, Aug. 2013.

[14] L. Mesin, "Volume conductor models in surface electromyography: Applications to signal interpretation and algorithm test," *Comput. Biol. Med.*, vol. 43, no. 7, pp. 953–961, Aug. 2013.

[15] L. Mesin and D. Farina, "A model for surface EMG generation in volume conductors with spherical inhomogeneities," *IEEE Trans. Biomed. Eng.*, vol. 52, no. 12, pp. 1984–1993, Dec. 2005.

[16] L. Mesin, M. Joubert, T. Hanekom, R. Merletti, and D. Farina, "A finite element model for describing the effect of muscle shortening on surface EMG," *IEEE Trans. Biomed. Eng.*, vol. 53, no. 4, pp. 593–600, Apr. 2006.

[17] L. Mesin, "Simulation of surface EMG signals for a multilayer volume conductor with triangular model of the muscle tissue," *IEEE Trans. Biomed. Eng.*, vol. 53, no. 11, pp. 2177–2184, Nov. 2006.

[18] L. Mesin and D. Farina, "An analytical model for surface EMG generation in volume conductors with smooth conductivity variations," *IEEE Trans. Biomed. Eng.*, vol. 53, no. 5, pp. 773–779, May 2006.

[19] L. Mesin, R. Merletti, and A. Rainoldi, "Surface EMG: The issue of electrode location," *J. Electromyogr. Kinesiol.*, vol. 19, no. 5, pp. 719–726, Oct. 2009.

[20] L. Mesin, "Real time estimation of generation, extinction and flow of muscle fibre action potentials in high density surface EMG," *Comput. Biol. Med.*, vol. 57, pp. 8–19, Feb. 2015.

[21] I. Talib, K. Sundaraj, C. K. Lam, J. Hussain, and M. A. Ali, "A review on crosstalk in myographic signals," *Eur. J. Appl. Physiol.*, vol. 119, no. 1, pp. 9–28, Jan. 2019.

[22] A. Merlo, M. C. Bó, and I. Campanini, "Electrode size and placement for surface EMG bipolar detection from the brachioradialis muscle: A scoping review," *Sensors (Basel)*, vol. 21, no. 21, p. 7322, 2021.

[23] I. Campanini, A. Merlo, C. Disselhorst-Klug, L. Mesin, S. Muceli, and R. Merletti, "Fundamental concepts of bipolar and high-density surface EMG understanding and teaching for clinical, occupational, and sport applications: Origin, detection, and main errors," *Sensors*, vol. 22, no. 11, p. 4150, May 2022.

[24] M. Besomi et al., "Consensus for experimental design in electromyography (CEDE) project: Electrode selection matrix," *J. Electromyogr. Kinesiol.*, vol. 48, pp. 128–144, Oct. 2019.

[25] A. Péter, E. Andersson, A. Hegyi, T. Finni, O. Tarassova, N. Cronin, H. Grundström, and A. Arndt, "Comparing surface and fine-wire electromyography activity of lower leg muscles at different walking speeds," *Frontiers Physiol.*, vol. 10, p. 1283, Oct. 2019.

[26] K. M. Barr, A. L. Miller, and K. B. Chapin, "Surface electromyography does not accurately reflect rectus femoris activity during gait: Impact of speed and crouch on vasti-to-rectus crosstalk," *Gait Posture*, vol. 32, no. 3, pp. 363–368, Jul. 2010.

[27] N. Jiang, K. B. Englehart, and P. A. Parker, "Extracting simultaneous and proportional neural control information for multiple-DOF prostheses from the surface electromyographic signal," *IEEE Trans. Biomed. Eng.*, vol. 56, no. 4, pp. 1070–1080, Apr. 2009.

[28] J. Zhao, Y. Yu, X. Wang, S. Ma, X. Sheng, and X. Zhu, "A musculoskeletal model driven by muscle synergy-derived excitations for hand and wrist movements," *J. Neural Eng.*, vol. 19, no. 1, Feb. 2022, Art. no. 016027.

[29] N. Zhao, B. Zhao, G. Shen, C. Jiang, Z. Wang, Z. Lin, L. Zhou, and J. Liu, "A robust HD-sEMG sensor suitable for convenient acquisition of muscle activity in clinical post-stroke dysphagia," *J. Neural Eng.*, vol. 20, no. 1, Feb. 2023, Art. no. 016018.

[30] Y.-K. Kong, M. S. Hallbeck, and M.-C. Jung, "Crosstalk effect on surface electromyogram of the forearm flexors during a static grip task," *J. Electromyogr. Kinesiol.*, vol. 20, no. 6, pp. 1223–1229, Dec. 2010.

[31] M. Solomonow, R. Baratta, M. Bernardi, B. Zhou, Y. Lu, M. Zhu, and S. Acierno, "Surface and wire EMG crosstalk in neighbouring muscles," *J. Electromyogr. Kinesiol.*, vol. 4, no. 3, pp. 131–142, Jan. 1994.

[32] M. M. Lowery, N. S. Stoykov, and T. A. Kuiken, "A simulation study to examine the use of cross-correlation as an estimate of surface EMG cross talk," *J. Appl. Physiol.*, vol. 94, no. 4, pp. 1324–1334, Apr. 2003.

[33] N. A. Dimitrova, G. V. Dimitrov, and O. A. Nikitin, "Neither high-pass filtering nor mathematical differentiation of the EMG signals can considerably reduce cross-talk," *J. Electromyogr. Kinesiol.*, vol. 12, no. 4, pp. 235–246, Aug. 2002.

[34] I. Campanini, A. Merlo, P. Degola, R. Merletti, G. Vezzosi, and D. Farina, "Effect of electrode location on EMG signal envelope in leg muscles during gait," *J. Electromyogr. Kinesiol.*, vol. 17, no. 4, pp. 515–526, Aug. 2007.
[35] L. Mesin, "Separation of interference surface electromyogram into propagating and non-propagating components," *Biomed. Signal Process. Control*, vol. 52, pp. 238–247, Jul. 2019.
[36] L. Mesin, "Non-propagating components of surface electromyogram reflect motor unit firing rates," *IEEE Access*, vol. 7, pp. 106155–106161, 2019.
[37] L. Mesin, "Inverse modelling to reduce crosstalk in high density surface electromyogram," *Med. Eng. Phys.*, vol. 85, no. 1, pp. 55–62, Nov. 2020.
[38] T. M. Vieira, A. Botter, S. Muceli, and D. Farina, "Specificity of surface EMG recordings for gastrocnemius during upright standing," *Sci. Rep.*, vol. 7, no. 1, p. 13300, Oct. 2017.
[39] L. Mesin, "Optimal spatio-temporal filter for the reduction of crosstalk in surface electromyogram," *J. Neural Eng.*, vol. 15, no. 1, Feb. 2018, Art. no. 016013.
[40] L. Mesin, "Nonlinear spatio-temporal filter to reduce crosstalk in bipolar electromyogram," *J. Neural Eng.*, vol. 21, no. 1, Feb. 2024, Art. no. 016021.
[41] L. Mesin, "Real time identification of active regions in muscles from high density surface electromyogram," *Comput. Biol. Med.*, vol. 56, pp. 37–50, Jan. 2015.
[42] C. M. Germer, D. Farina, L. A. Elias, S. Nuccio, F. Hug, and A. Del Vecchio, "Surface EMG cross talk quantified at the motor unit population level for muscles of the hand, thigh, and calf," *J. Appl. Physiol.*, vol. 131, no. 2, pp. 808–820, Aug. 2021.
[43] C. Chen, Y. Yu, X. Sheng, D. Farina, and X. Zhu, "Simultaneous and proportional control of wrist and hand movements by decoding motor unit discharges in real time," *J. Neural Eng.*, vol. 18, no. 5, Oct. 2021, Art. no. 056010.
[44] M. Gazzoni, B. Afsharipour, and R. Merletti, "Surface EMG in ergonomics and occupational medicine," *Surf. Electromyography, Physiol.*, vol. 31, pp. 361–391, Apr. 2016.
[45] A. D. Vigotsky, I. Halperin, G. J. Lehman, G. S. Trajano, and T. M. Vieira, "Interpreting signal amplitudes in surface electromyography studies in sport and rehabilitation sciences," *Frontiers Physiol.*, vol. 8, p. 985, Jan. 2018.
[46] G. I. Papagiannis, A. I. Triantafyllou, I. M. Roumpelakis, F. Zampeli, P. Garyfallia Eleni, P. Koulouvaris, E. C. Papadopoulos, P. J. Papagelopoulos, and G. C. Babis, "Methodology of surface electromyography in gait analysis: Review of the literature," *J. Med. Eng. Technol.*, vol. 43, no. 1, pp. 59–65, Jan. 2019.
[47] I. Campanini, C. Disselhorst-Klug, W. Z. Rymer, and R. Merletti, "Surface EMG in clinical assessment and neurorehabilitation: Barriers limiting its use," *Frontiers Neurol.*, vol. 11, p. 934, Sep. 2020.
[48] P. Zhou, N. L. Suresh, M. M. Lowery, and W. Z. Rymer, "Nonlinear spatial filtering of multichannel surface electromyogram signals during low force contractions," *IEEE Trans. Biomed. Eng.*, vol. 56, no. 7, pp. 1871–1879, Jul. 2009.
[49] D. Farina, L. Mesin, S. Martina, and R. Merletti, "A surface EMG generation model with multilayer cylindrical description of the volume conductor," *IEEE Trans. Biomed. Eng.*, vol. 51, no. 3, pp. 415–426, Mar. 2004.
[50] A. J. Fuglevand, D. A. Winter, and A. E. Patla, "Models of recruitment and rate coding organization in motor-unit pools," *J. Neurophysiology*, vol. 70, no. 6, pp. 2470–2488, Dec. 1993.
[51] S. Andreassen and L. Arendt-Nielsen, "Muscle fibre conduction velocity in motor units of the human anterior tibial muscle: A new size principle parameter," *J. Physiol.*, vol. 391, no. 1, pp. 561–571, Oct. 1987.
[52] P. Contessa and C. J. D. Luca, "Neural control of muscle force: Indications from a simulation model," *J. Neurophysiology*, vol. 109, no. 6, pp. 1548–1570, Mar. 2013.
[53] M. Raggi, G. Boccia, and L. Mesin, "Reduction of crosstalk in the electromyogram: Experimental validation of the optimal spatio-temporal filter," *IEEE Access*, vol. 11, pp. 112075–112084, 2023.
[54] L. Mesin, F. Tizzani, and D. Farina, "Estimation of motor unit conduction velocity from surface EMG recordings by signal-based selection of the spatial filters," *IEEE Trans. Biomed. Eng.*, vol. 53, no. 10, pp. 1963–1971, Oct. 2006.
[55] D. Farina, L. Mesin, and S. Martina, "Advances in surface electromyographic signal simulation with analytical and numerical descriptions of the volume conductor," *Med. Biol. Eng. Comput.*, vol. 42, no. 4, pp. 467–476, Jul. 2004.
[56] D. Farina and A. Rainoldi, "Compensation of the effect of sub-cutaneous tissue layers on surface EMG: A simulation study," *Med. Eng. Phys.*, vol. 21, no. 6, pp. 487–497, Jul. 1999.
[57] D. Farina and R. Merletti, "Methods for estimating muscle fibre conduction velocity from surface electromyographic signals," *Med. Biol. Eng. Comput.*, vol. 42, no. 4, pp. 432–445, Jul. 2004.
[58] M. J. T. Tan, H. R. Kasireddy, A. B. Satriya, H. A. Karim, and N. AlDahoul, "Health is beyond genetics: On the integration of lifestyle and environment in real-time for hyper-personalized medicine," *Frontiers Public Health*, vol. 12, 2025, Art. no. 1522673, doi: 10.3389/fpubh.2024.1522673.

LUCA MESIN received the Graduate degree in electronics engineering and the Ph.D. degree in applied mathematics from the Politecnico di Torino, Italy, in 1999 and 2003, respectively. He is currently an Associate Professor in biomedical engineering and a Supervisor of the Mathematical Biology and Physiology Group, Department of Electronics and Telecommunications, Politecnico di Torino. His current research interests include biomedical image and signal processing and mathematical modeling.